Universidade de Aveiro Departamento de Ambiente
2010

Hydrodynamical and Biogeochemical modeling study of Sado Estuary

Estudo de Modelação Hidrodinâmica e Biogeoquímica do Estuário do Sado

Dissertação apresentada à Universidade de Aveiro para cumprimento dos requisitos necessários à obtenção do grau de Mestre em Ciências do Mar e Zonas Costeiras, realizada sob a orientação científica do Prof. Dr. João Miguel Dias, Professor Auxiliar do Departamento Física da Universidade de Aveiro e co-orientação do Doutor Nuno Vaz, Investigador Auxiliar do Centro de Estudos do Ambiente e do Mar (CESAM).

Dedico este trabalho em especial à minha família (Jorge, Miquelina, Jorge Miguel e Sofia, Avô Zé e Avó Geninha) e ao meu Bu por todo o apoio.

o júri

presidente

Prof. Dr. Filomena Maria Cardoso Pedrosa Ferreira Martins
Professora Associada do Departamento de Ambiente da Universidade de Aveiro

Prof. Dr. João Miguel Sequeira Silva Dias
Professor Auxiliar do Departamento de Física da Universidade de Aveiro

Doutor Nuno Vaz
Centro de Estudos do Ambiente e do Mar (CESAM) da Universidade de Aveiro

Doutor Paulo Miguel Chambel Filipe Lopes Teles Leitão
Consultor da Hidromod-Modelação em Engenharia, Lda.

agradecimentos

Ao Orientador João Miguel Dias, sem si não teria me inscrito nem conhecido o Mestrado em Ciências do Mar e Zonas Costeiras, nem teria feito a tese nesta área. Obrigado pela paciência e ajuda dada ao longo da elaboração deste trabalho.

Ao Co-Orientador Nuno Vaz, sem ti teria sido impossível fazer esta viajem, por toda a orientação, sacrifício, horas perdidas e mão amiga que me deste um MUITO OBRIGADO sentido.

Aos meus amigos de Setúbal e do coração: Silvia, Lena, Zé, Anilena, Bruninho e Rita, Fanecas, Leitão e Di, João e Carolina, Bonaparte, Ângela, Cátia, Rocha, e a todos os que me esqueci um muito OBRIGADO por me aturarem nas minhas infindáveis crises de apoplexia nervosa e cerebral!

Aos meus Pais e Avós Maternos que tornaram isto possível!

Ao meu Bu que me deu sempre a mão, o pé e tudo mais quando o chão pareceu desaparecer…

A todos os que tiveram a paciência de me aturar e encorajar ao longo deste percurso que parecia não ter fim, MUITO OBRIGADO, sem vocês teria sido impossível terminar esta jornada.

Em especial ao meu avô Zé que durante a elaboração deste trabalho passou a iluminar-me, a inspirar-me e a guiar-me das estrelas…

palavras-chave Estuário do Sado, Hidrodinâmica, Coliformes fecais, modelo MOHID-2D

resumo

O estuário do Sado encontra-se inserido no parque natural da Arrábida junto à cidade de Setúbal. A baixa descarga de água doce proveniente do rio Sado, a maré mesotidal ao longo do estuário e as fortes correntes que aqui se observam tornam o estuário um sistema bem misturado, controlando o tempo de residência e determinando assim os padrões de traçadores conservativos e não conservativos. A dinâmica salina no interior deste tipo de sistemas é muito importante, uma vez que a salinidade pode ser considerada um traçador natural, permitindo a compreensão da dinâmica de outros traçadores. Num sistema como este, é também importante analisar a qualidade da água, determinando a propagação de coliformes provenientes de estações de descargas seleccionadas e analisando a sua relação com as estruturas hidrográficas do estuário.

Neste estudo, um modelo hidrodinâmico bidimensional é implementado para o estuário do Sado, com o objectivo de estudar os padrões horizontais de salinidade, bem como a propagação de coliformes fecais com origem em estações de esgoto locais. São avaliadas condições distintas de maré (maré-viva, maré-morta), diferentes fases da mesma (enchente e vazante) e descargas características do caudal fluvial (baixo ($2m^3s^{-1}$), médio ($50m^3s^{-1}$) e elevado ($200m^3s^{-1}$)). O modelo usado neste estudo foi o MOHID-2D (www.mohid.com), um modelo marinho que utiliza a aproximação de águas pouco profundas para estudar sistemas verticalmente homogéneos, como é o caso do estuário do Sado. O domínio do modelo abrange toda a área do estuário, usando a linha de costa e topografia de fundo realista.

Os resultados do modelo são explorados de modo a avaliar as diferenças de salinidade entre enchente e vazante, maré-viva e maré-morta e baixo, médio e elevado caudal fluvial. Posteriormente foi ainda estudada a propagação de coliformes fecais nas condições anteriormente referidas. As previsões do modelo em termos de velocidade e nível de maré são comparadas com observações *in situ,* revelando a capacidade do modelo em reproduzir adequadamente a propagação de maré ao longo do estuário do Sado.

Quando o caudal fluvial é fraco ($2m^3s^{-1}$), a hidrografia do estuário é claramente dominada pela maré, quando este é elevado ($200m^3s^{-1}$) os parâmetros horizontais de salinidade dentro do estuário são determinados por um balanço entre o efeito da maré e do caudal fluvial. Neste caso é perceptível a divisão do estuário em três regiões: marinha, de mistura e de água doce. Nesta última a dinâmica do estuário é principalmente modulada pela descarga de água doce proveniente do rio.

Apesar da dinâmica estuarina, as concentrações de coliformes fecais mostraram estar confinadas a pequenas áreas junto às estações de descarga de esgoto, sendo detectadas concentrações bastante baixas em zonas mais afastadas dos pontos de descarga e ao longo do estuário.

keywords Sado estuary, Hydrodynamics, Fecal coliform, MOHID-2D model

abstract

The Sado estuary is located in the surrounding area of an important Portuguese natural park (Arrábida Natural Park) near the city of Setúbal. The low freshwater discharge from Sado River, the mesotidal tide along the estuary and the strong currents observed turn the estuary a well-mixed system, controlling the estuarine residence time, and therefore determining the patterns of conservative and non-conservative tracers. The salt dynamics inside this kind of system is very important, since salinity may be considered a natural tracer, allowing the comprehension of the dynamics of other conservative tracers. In such a system is also important to analyze the water quality determining the coliforms propagation from selected discharge stations and analyzing its relation with the estuarine hydrographic features.

In this study, a two-dimensional hydrodynamic model is implemented for the Sado estuary in order to study the horizontal patterns of salinity, as well as the propagation of fecal coliforms from sewage stations, both under different tidal and freshwater forcing conditions. The model used in this study is Mohid-2D (www.mohid.com), a marine model that uses the shallow water approximation to study vertically homogeneous systems like the Sado estuary. The model domain includes the whole area of the estuary, using a realistic coastline and bottom topography

The model results are explored in order to evaluate salinity differences between flood and ebb, spring and neap tide, and low ($2m^3s^{-1}$), medium ($50m^3s^{-1}$) and high ($200m^3s^{-1}$) river inflow. Moreover, the propagation of fecal coliforms from sewage stations is also studied in light of different tidal and freshwater inflow conditions. Sea surface height and velocity model outputs are compared to *in-situ* data, revealing the model skill in reproducing the tidal propagation along the Sado estuary.

When the river inflow is weak ($2m^3/s$), the hydrography of the estuary is clearly tidal dominated but when the river inflow is high ($200m^3/s$), the horizontal patterns of salinity inside the estuary are determined by a balance between tide and river inflow effects. In this case is found a classic division of the estuary in three distinct regions: marine, mixing and freshwater. In this last region the estuary dynamics is mainly modulated by the freshwater discharge.

Despite the significant estuarine dynamics, the concentration of fecal coliforms was found confined to small areas close to the discharge points. These organisms were found to affect only a restricted area near the sewage stations, with low concentrations found far the discharge points along the estuary.

Especialmente a Ti,
Porque continuas a ser o meu Farol…

GENERAL INDEX

FIGURE INDEX

TABLE INDEX

I. INTRODUCTION

Estuary Definition: "*An estuary is defined as a semi-enclosed coastal body of water which has a free connection with the open sea and within which sea water is measurably diluted with freshwater derived from land drainage*"[Cameron and Pritchard, 1963].

An estuary is a partially enclosed body of water along the coast, where freshwater from rivers and streams meet and mix with salt water from the ocean. In its margins and low lands, there are places of transition from land to sea, and despite the tidal influence, they are protected from the full force of the ocean waves, winds, and storms by landforms such as barrier islands and/or peninsulas. More than 60% of the world population live nearby estuaries, and it is here that is produced and explored a huge part of the marine resources [Pinho, 2000]. Tourism, fisheries, and other commercial activities prosper on the wealth of natural resources that estuaries supply. The protected coastal waters of estuaries also support important public infrastructures, serving as harbours vital for shipping, transportation, and industry. Therefore these regions are subjected to extremely high social and environmental stress.

1.1. Estuarine dynamics

Estuarine studies normally present a high degree of difficulty, once these aquatic systems combine complex geometry and hydrodynamic circulation patterns, being subjected and modified by natural and anthropogenic forcing. In fact, estuaries are subjected to tidal, fluvial discharges and winds forcing, with specific characteristics which modulates the sedimentary transport patterns that shape their morphology (Figure 1). There is a great diversity in the interface characteristics that are different in each estuary, depending on the type of tides, river runoff, and other factors that interact directly with the bathymetry and geometry [Dyer, 1997].

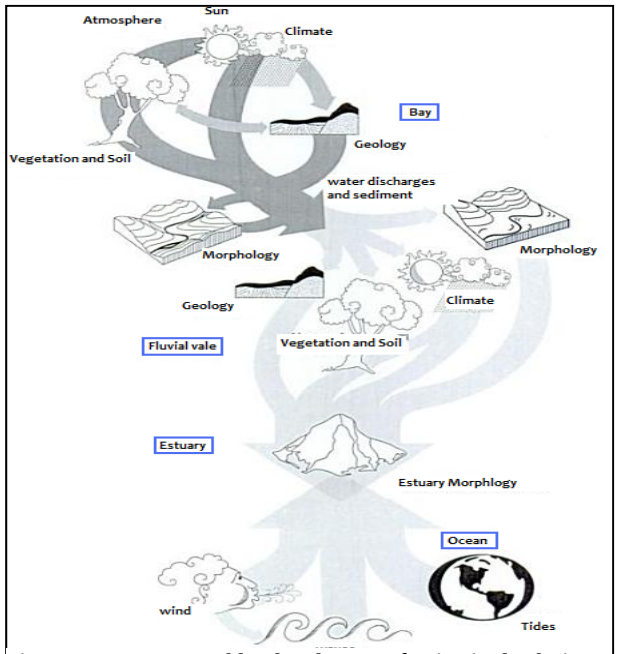

Figure 1 - Processes and local and remote forcing in the drainage bay and in the adjacent ocean, determinant for the characteristics and dynamics of an estuary (source: Principios de Oceanografia de Estuários, Miranda&Castro&Kjerfve 2002)

The intertidal areas are of extreme importance once they support not only local fish and shellfish populations that are harvested commercially and recreationally, but also because they provide food and habitat to a large community of organisms, which are the base of the marine chain food. These are low water areas,

and when the rivers discharge high amounts of fine materials it is in these areas that they are mostly cached forming zones of low depth normally rich in organic matter by drainage or accumulation.

Tide: *"The periodic variation in the surface level of the oceans and of bays, gulfs, inlets, and estuaries, caused by gravitational attraction of the moon and sun"* [Middle English, from Old English, division of time; see in Indo-European roots].

The two most important estuarine forcing affecting meso and macrotidal estuaries are the tidal motion and river runoff. The importance of the second depends on its own river runoff value, velocity and associated load concentration. The tidal force induces currents opposite to the fluvial current throughout the flood; so during the outflow periods the fluvial current receives a great reinforcement by the ebb current. Reaching the estuary, the fluvial current weakens because of the decrease of the slope and resistance given by the ocean water, and becomes null, that is: the inflow tide enters along the fluvial channel until variable distances, depending on river runoff and tidal amplitude. Entering along the estuary or tidal channel, the inflow tidal amplitude diminishes until it becomes null. In maximum high tide, the sea level is higher than the hydrometric level of the river waters. On the other hand, in the maximum low tide, the river hydrometric level is much higher than the sea level. This occurs because the sea water joins the river water during the inflow. It is due to the mentioned slope that during the outflow there is a large discharge which can reach high velocities.

The maximum high tides (spring tides) occur when the moon and sun are directly aligned with Earth, meaning that the gravitational pull on Earth's water is reinforced by this alignment. The lowest high tides (neap tides) occur when the Moon and Sun are at right angles to each other, so that their gravitational pull on Earth's waters originates from two different directions is mitigated. Tides vary greatly from region to region and are influenced by the topography, storms (meteorological effects), and water currents [The American Heritage® Science Dictionary Copyright © 2005 by Houghton Mifflin Company] (Figure 2).

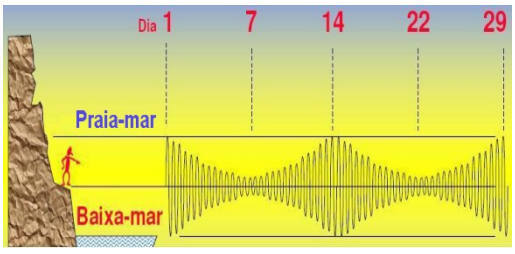

Figure 2 - Illustration of tide amplitude (high tide (PM) and low tide (BM))

Although there have been identified over than 400 tide components, the use of the first four (M2+K1+S2+O1) explain about 83% of the total tide amplitude [http://www.aprh.pt/rgci/glossario/mare.html]. The result of the two high and two low tides during one day is designated by semi-diurnal tide, when there is only one high tide and one low tide, the resulting tide is designated by diurnal tide.

The importance of the diurnal and semi-diurnal tidal constituents can be evaluated by the adimensional Form Number (N_f) defined by A. Courtier in 1938 [Defant, 1960]: $\boldsymbol{N_f} = \frac{K_1+O_1}{M_2+S_2}$

Tides can be classified by the period given by form number (N_f), see Table1:

Table 1 – Tide classification (Miranda *et al.* 2002)

$0 < N_f < 0.25$	Semi-diurnal
$0.25 < N_f < 1.5$	Mixed, predominant semidiurnal
$1.5 < N_f < 3.0$	Mixed, predominant diurnal
$N_f > 3.0$	Diurnal

1.2. Fecal coliforms

Significance: *Fecal Coliform bacteria indicate the presence of sewage contamination of a waterway and the possible presence of other pathogenic organisms* (*http://www.switzerland.k12.in.us/watershed/fecal.html*).

Bacteria are one celled organisms that can only be seen with very powerful microscope instrumentation. Bacteria can be found in the air, water, and soil. Fecal coliform bacteria are a group of bacteria that are passed through the fecal excrement of humans, livestock and wildlife. A specific subgroup of this type of bacteria is the *Eschericia coli*. These organisms may be separated from the total coliform group by their ability to grow at high temperatures. Bacteria reproduce rapidly if optimal conditions are available (tide + temperature + solar radiation). By growing and counting colonies of fecal coliform bacteria from a sample of stream water, it can be approximately determined how many bacteria were originally present. Fecal coliform bacteria can be found in rivers through direct discharge of waste from mammals and birds, from agricultural and storm runoff, and from untreated human sewage. The presence of fecal contamination is an indicator of a potential health risk for individuals exposed to this water.

Reduction/treatment of fecal coliform in wastewater may require the use of chlorine and other chemicals disinfectant. Such materials may kill the fecal coliform and disease but they also kill bacteria essential to the aquatic environment balance, endangering the survival of species dependent on those bacteria. Therefore, higher levels of fecal coliform require higher levels of chlorine, threatening those aquatic organisms [Doyle and Erickson, 2006]. Thus the importance of fecal coliform studies, particularly when attempting to combine new ways of treatment and containment of possible blooms is high.

There are legislated values in each country for the presence of fecal coliforms in water. The legislated standard values in Portugal are presented in Table2:

Table 2 - Legislated values in Portugal for the presence of fecal coliforms in water
(fonte: DL nº236/98, Anexo XV, Qualidade das águas balneares)

Parameters	Maximum admissible value (MVA)	Maximum value recommended (MVR)
Total Coliforms (nº/100ml)	10.000	500
Fecal Coliforms (nº/100ml)	2.000	100

1.3. Literature survey

In this section a brief literature survey on numerical modelling and fecal coliform studies is presented. The correct management of coastal environmental problems requires integrated technical and scientific tools, based on numerical models, field data acquisition and Earth observation, which can prospective a precise analysis of the occurring phenomena, previewing its evolution and supporting the knowledge of coastal processes. Nowadays, the implementation of numerical models is recurrent in many areas. Numerical models are developed not only to reinforce *in situ* studies/analysis but also when temporal and/or spatial coverage isn't quite adequate. Other circumstances, in which estuaries can benefit from modeling, are the comprehension of its complex dynamics, processes and the response to forcing factors.

Meller [2004] developed a study in Brasil with the main purpose of simulating integrated hydrodynamical drainage system of the Santa Maria-RS. The main goal of the study was to evaluate the urban drainage system of Residential Park Alto da Colina, which presents flood points during high storms, using monitoring data. Through the use of rainfall runoff and hydrodynamic 1D model, included in the package MOUSE v.2003, current problems concerning the inefficiency of the drainage system and aiming solutions for the urban drainage planning in the area were analyzed.

Other issue is the thermohaline dynamics that during the last decades has been studied in several estuarine systems worldwide. Ecologically, this has a great importance, once the studies can provide knowledge about system changes and the effects on the surrounding fauna. The salt fluxes and temperature changes can have disturbing effects on the communities behaviour, once the bases of the trophic chain is affected and, consequentially, the whole chain will suffer transformations. Studies of estuarine response to changes in river flow input, in terms of both their time scale [Kranenburg, 1986; MacCready, 1999] and magnitude [Officer and Kester, 1991; Gibson and Najjar, 2000; Monismith *et al.*, 2002] occupied much of the literature.

As for the model MOHID, it has been applied to several different coastal and estuarine areas and has shown its ability to simulate complex features of the water flows. Along the Portuguese coast, several environments have been studied, from river mouths (Douro and Mondego) to coastal lagoons (Ria de Aveiro [Trancoso *et al.*, 2005; Vaz *et al.*, 2005a] and Ria Formosa) and broader estuaries (Tagus [Braunschweig *et al.*, 2003] and Sado estuaries [Martins *et al.*, 2001]). Moreover, the model has been implemented to simulate the Galician

Rias hydrodynamics (Ria de Vigo [Taboada *et al.*, 1998; Montero, 1999], Ria de Pontevedra [Villarreal *et al.*, 2002]). Far from the Atlantic coast of the Iberian Peninsula, some European estuaries have been studied (Western Scheltd, Holland, and Gironde, France [Cancino and Neves, 1999] and Hellingford [Leitão, 1996]) as well as some coastal estuaries in Brazil (Santos and Fortaleza).
The hydrodynamic module aims to be a numerical tool oriented to help understanding biogeochemical processes and resolve ecological problems associated with human activity.

In Portugal, Rebordão [2008] analysed the energetic potential of the tidal flux energy in the Lima Estuary through the application of the numerical model ADCIRC. Vaz *et al.* [2007] studied the hydrodynamics of Ria de Aveiro applying MOHID-2D numerical model; Vaz *et al* [2009] studied the Espinheiro Channel hydrodynamic and hydrographic features in order to assess the Channel's vertical structure under different tidal and river inflow conditions. Duarte [2006] applied MONDEST (2D-H) to the Mondego River with the objective of developing a hidroinformatic methodology for the integrated study of the interaction between hydrodynamics and estuarine waters ecological quality modifications. Dias. *et al.*, [2009] described the application of hydrodynamic (ELCIRC) and transport (VELA and VELApart) models to the Ria Formosa lagoon (Portugal) to study the impact of the relocation of the Ancão Inlet viewing tidal currents, residual velocities and the tidal prism across the bar. Oliveira *et al.* [2006] studied the hydrodynamics, the salinity intrusion and stratification in the Guadiana estuary applying ADCIRC shallow water model for depth-averaged flow simulations and ELCIRC 3D baroclinic model for salinity intrusion and stratified conditions. Duarte [2006] studied the hydrodynamics influence in estuarine systems subjected to eutrophication, (Mondego river case) applying MONDEST model in order to estimate and evidence the influence of residence time, current velocity and salinity spatial distribution on eutrophication process of Mondego estuary at different simulated scenarios and discharges characteristics.

In the specific case of the Sado estuary a few studies have been made. Martins *et al.* [1998, 2002] applied MOHID-2D to study the environmental impact associated to dredging works in the Setubal Harbour, aned the use of sedimentary transport coupled to the hydrodynamical model showed to be a sound methodology. Martins *et al.* [2001] and Neves *et al.* [2004], applied a 3D baroclinic hydrodynamic model coupled to two transport models, one with langrangian formulation and the other with eulerian, to study an ecological approach (the impact produced by the raise of nutrients on the primary production), assuming that the estuary has some sensitivity to the raise of nutrients introduced by the river producing eutrophication. INAG/MARETEC/IST [2002] conducted a study in *Mondego, Tejo and Sado* estuaries with a water quality approach and concluded that modeling proved to be a useful tool to overcome the difficulties associated with the lack of information and to its uneven distribution in space and time. Model results were also very useful for assessing the representativeness of data for explaining the ecological functioning of the estuaries and the spatial meaning of the average values defined for each estuary. The main goal of Caeiro *et al.* [2003] was to design a robust spatial sampling strategy for the Sado Estuary. Sampling was integrated into a GIS within a digitized Sado Estuary boundary, allowing future integration of environmental monitoring and management information. This boundary was digitized with the tidal knowledge acquired, which will also permit accurate studies of shoreline evolution and changes. These studies are of particular importance with regard to sea level

changes related to natural or anthropogenic climate changes and any consequent variations in estuarine morphology.

In terms of fecal coliform, many studies have been conducted around the world. Wilkinson *et al.* [1995] performed a study in Mid-Wales on the Afon Rheidol, which flows through Aberystwyth into the Irish Sea, implementing a model to study fecal coliform dynamics in streams and rivers, based on the mass-balance plan adopted by Jenkins [1984]. The preliminary results of the conceptual model allow simulations of entrainment from any previous flow to be simulated by rapid depletion of discrete storage areas when subject to entrainment. Steetsa and Holden [2003] in Arroyo Burro lagoon in Santa Barbara - California, used a numerical modeling approach to study the runoff-associated fecal coliform fate and transport through a coastal lagoon, but the model itself contained model parameter values that were site and season-specific. The results suggested that there were seasonally varying roles for coastal lagoons in mediating fecal coliform contamination to coastal waters and pointed for coastal lagoons or marshes to be also a source of high indicator organism concentrations in coastal waters. Neill [2004] applied a microbiological index to Suir/Barrow/Nore (Ireland) estuary and Waterford Harbour and concluded that microbiological indices are an effective mean of appraising or assessing the bacterial counts for total coliform and E. coli in estuarine waters–covering the full salinity range. The indices are used to decide if the bacterial counts for total coliforms and E. coli. The indices are particularly useful to evaluate the bacterial counts for total coliform and E. coli in estuaries that receive direct discharges of sewage. Servais *et al.* [2007] developed a study program concerning the microbiological water contamination of the rivers of the Seine drainage network. As a result, a module describing the dynamics of fecal bacteria has been developed and embedded within a hydro-ecological model, describing the functioning of the rivers of the whole watershed (the SENEQUE model). As major conclusion, once validated, such models can be used for testing predictive scenarios and, thus, can be a useful tool for the management of microbiological water quality at the scale of the whole basin. Randall [2000] conducted a study to determine total maximum daily Load (TMDL) for fecal coliform bacteria in the waters of Duck Creek in Mendenhall Valley, Alaska, using the numeral model Storm Water Management Model (SWMM) and simulated the quantity and quality of runoff produced by storms in urban watersheds [USEPA, 1997]. SWMM allowed the representation of mixed-land-use watersheds using continuous simulation based on observed meteorological conditions. At the sub-watershed scale, SWMM provides for evaluation of in-stream conditions, allowing for direct comparison with the relevant water quality standards.

For the specific case of Sado estuary Mourão *et al.* [2004], describe the application of the indicators framework DPSIR - Driving Forces-Pressures-State-Impact-Response in a Geographical Information System (GIS) context, to the Sado estuary (Portugal). The preliminary results of the quantitative indicators, allowed discussing the indicator's information and limitations. These results confirm that the Setubal sub-watershed contains clustered populated areas near the city of Setúbal, where are located the major ports and industries complexes, and there are agriculture and aquaculture activities. Due to this high social and economic pressure, a high environmental impact is expected in the north margin of the Sado Estuary.

1.4. Motivation

Estuaries and surrounding areas are highly dynamic systems that respond to natural and anthropogenic factors. They have a great importance not only because they are highly rich in flora and fauna but because they support a great amount of recreation and economical human activities.

Due to high population density and presence of industrial complexes, estuaries are subjected to huge human stress. In order to fully characterize these systems it is necessary to have an extensive data set (temporal and spatial). However, field measurements are not enough due to human and resource limitations and because estuaries are aquatic systems that combine complex geometry and hydrodynamical circulation patterns. Therefore the development of numerical models becomes important to study the estuary characteristics, fill in the existing gaps in field data coverage and to produce useful tools to environmental management.

The main purpose of this work was to research the Sado estuary processes using a high resolution model: MOHID – water modelling system (www.mohid.com), in order to analyse the hydrodynamics (bottom friction and river inflow effects), saline horizontal patterns and, in addition, to study fecal coliform dispersion in order to assess the estuary water quality.

1.5. Objective

The major objectives of this work are to study the hydrodynamics and dispersion of fecal coliforms in the Sado estuary, using the numerical model MOHID (www.mohid.com). This study was focused on the analysis of hydrodynamic patterns and fecal coliforms distribution under different tidal and freshwater scenarios. The following sections describe the model, methodology and scenarios used in this work. Due to the physical characteristics of the estuary the model will be used in a 2D mode (intense tidal motion and low freshwater inflow).

1.6. Study area

The Sado estuary is located 40 km south of Lisbon, Portugal (Figure 3). It is about 20 km long and 4 km wide and its average depth is about 8 m. The Sado River discharges into a tidal estuary with an area of around 180 km^2 with a complex morphology. Intertidal areas and sand/mud banks separates a north and a south channel near the city of Setúbal [Martins *et al.* 2002].

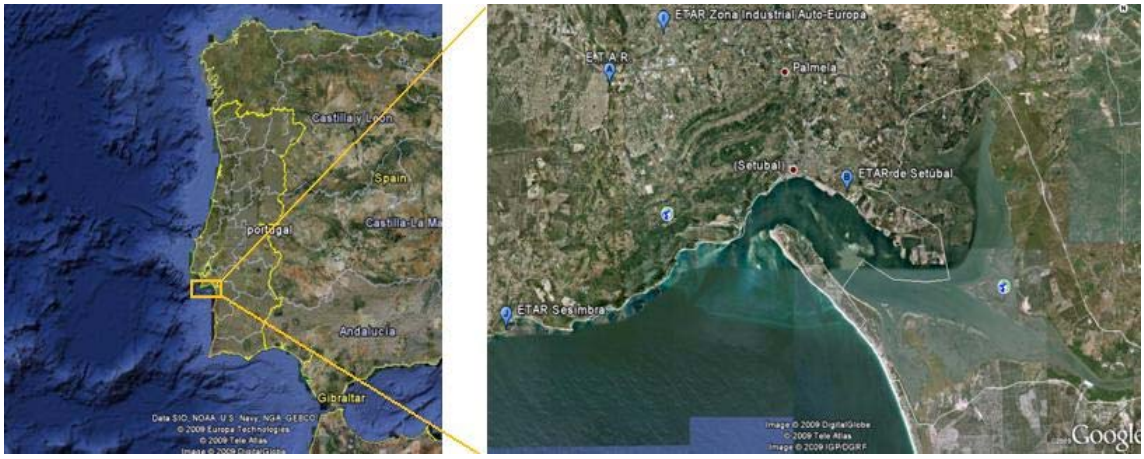

Figure 3 - Study area, Sado estuary (fonte: www.googlemaps.com).

Estuaries can, generally, be divided in a upper and a lower parts as suggested by Wollast and Juillet [1978], based on the temperature and salinity distributions; and divided in three areas [Kjerfve, 1989]: (a) a marine or lower estuary, (b) a middle estuary where the mixing between the fresh and salt water occurs and an (c) upper or fluvial estuary characterized by freshwater but still subject to a daily tidal action. The delimitation of these areas is dynamic and can change seasonally (or in lower time scales) due to the tide, winds or the river inflow [Kjerfve, 1990; Miranda *et al.*, 2002].

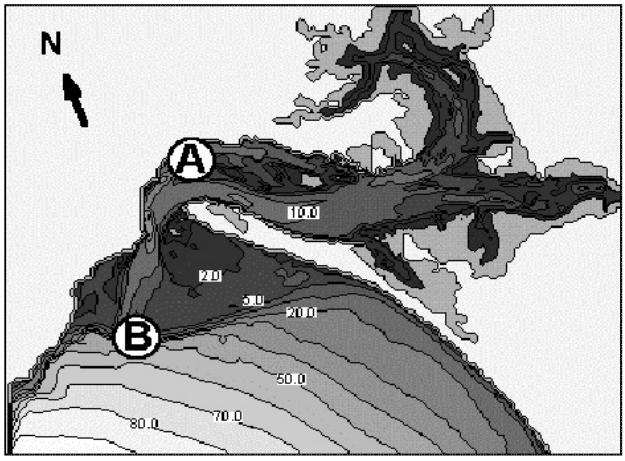

Figure 4 - Sado estuary bathimetry, INAG image (www.inag.pt)

The upper estuary has two main channels: the Alcácer channel, (35k m long and 700 m wide, with an average depth of 5 m and about 80% of total freshwater inflow), and the Marateca channel on the north side (about 10% of total freshwater inflow). The middle estuary (5 km wide, 20 km long and 10 m depth) is a wide embayment with a large salt marsh on the southern side. The connection with the ocean is made through a deep and narrow channel. The lower estuary behaves as a coastal lagoon, with small freshwater influence, while the upper river channel behaves as a typical long and narrow estuary characterized by the freshwater input (Figure 4). A 14 m depth navigation channel is dredged across the platform located outside the estuary. This channel intensifies the ebb stream and modifies the flow pattern in the adjacent slope between the 5 m and the 20 m isobaths.

The low average depth, strong tidal currents and low freshwater discharge turn the Sado estuary a well mixed estuary. The Sado estuary is a mesotidal estuary with an average spring tidal range of 2.7 m. The tide is semidiurnal, with amplitude of about 1.6 m in spring tides and 0.6 m in neap tides and with sea surface heights in the inlet between 3.2 m (spring tide) and 1.2 m (neap tide). The most important tidal constituents are the M_2 and the S_2. At the mouth, their amplitudes are 0.98 m and 0.35 m, respectively, being amplified upstream.The annual average river runoff is ± 40 m^3s^{-1} [Vale *et al.*, 1993], presenting strong seasonal variability, with daily medium values minor than 1 m^3s^{-1} in summer and higher than 150 m^3s^{-1} in winter time [Cabeçadas, 1993]. Circulation is mainly tidally driven [Martins *et al.*, 2001]. At the upper reaches, intertidal mudflats and salt marshes occupy about 1/3 of the estuary. The primary production is limited by nutrients and by the phytoplankton and zooplankton interaction. The water residence time, inside each part of the estuary, is of the order of one week, resulting in strong mixing between different areas, with deposition and mineralization of particulate organic matter in the shallow intertidal areas, being the medium value used of one month [OSPAR Maretec Report in Sado estuary, 2002]. Table 3 summarizes some of the main physical properties of the Sado estuary.

Table 3 - Main physical properties of Sado Estuary

Parameter Value	
Volume	500×10^6 m^3
Total area	180 km^2
River Discharge	40 m^3 s^{-1}
Tidal range	2.7 m
Typical residence time	1 month

For a better understanding of the transport processes inside the estuary, the residual circulation is also presented. The residual circulation is the average flow and gives an idea of the preferential transport of any property discharged in the estuary. To obtain the residual velocity, the model must run over a period of time much longer than the time periods associated to the variability of the transient flow. The residual flux can be defined as the average of the transient water flux per unit of length (m^2/s). The result was obtained by integrating the velocities in Sado Estuary over a period of 15 days. The pattern shows an important recirculation inside the estuary, right in front of the town of Setúbal. This recirculation shows that in the northern channel there is more water flowing during flooding than during ebb and that in the southern channel it happens the reverse. Integrating the flux all over across section, one would get the river discharge, and the corresponding residual velocity would be very small (of the order of 1 mm/s). This eddy shows residual velocities in the order of 10 cm/s, showing that the tidal mixing is the most efficient mechanism for estuary water renewal. In a more linear system, both flood and ebb velocities would be lower. This eddy is quite important for the residence time, generating much shorter residence times in the lower estuary, through the generation of intense mixing. Similar eddies further inside the estuary also generate high mixing of water from different parts of the estuary. Through that mixing, those eddies also contribute to reduce the residence time of the water inside the estuary [Neves & Martins 2004].

II. METHODS

2.1. Model description

The MOHID Water Modelling System has been programmed using an object oriented approach to facilitate the integration of new processes and models. The numerical algorithms used are based on the finite volume approach, a flux-driven strategy that facilitates the coupling of different processes and allows conservation of mass and momentum and is programmed in ANSI FORTRAN 95 [Braunschweig *et al.*, 2004]. MOHID I/O formats are in the form of time series at given point (ASCII files) and/or matrix data in HDF5 binary format. There are several tools to produce, convert to and from, and to visualize these files, such as MOHID GIS and MOHID GUI [Braunschweig *et al.*, 2005].

The three-dimensional (3D) water modelling system MOHID includes a baroclinic hydrodynamic module for the water column, sediments and the correspondent eulerian and lagrangian transport modules. Parameters and processes involving non-conservative properties are object of specific modules (e.g. turbulence module, water quality, ecology and oil transformation). The turbulence module uses the GOTM turbulence model [Burchard *et al.* 1999]. MOHID is in constant development and its website can be found at: www.mohid.com.

2.1.1. The numerical model equations

MOHID solves the three-dimensional incompressible primitive equations. Hydrostatic equilibrium is assumed as well as the *Boussinesq and Reynolds* approximations. All the equations below have been derived taken into account these approximations. A detailed derivation of the model equations was presented in several studies referred by Santos [1995], Martins *et al.* [2001], Leitão [2003]. The ***hydrostatic approximation*** is assumed with:

$$\frac{\partial p}{\partial z} = -\rho g \tag{2.1}$$

where g is gravity and ρ is density. If the atmospheric pressure p_{atm} is subtracted from p, and density ρ is divided into a constant reference density ρ_0 and a deviation component ρ', after integrating from the free surface η to the depth z where pressure is calculated, it is obtained:

$$p(z) = p_{atm} + g\rho(\eta - z) + g\int_z^\eta \eta\rho' dz \tag{2.2}$$

By using the Boussinesq approximation - where the density variation is small (≈3%), the horizontal pressure gradient in the x_i directions can be divided into:

$$\frac{\partial P}{\partial x_i} = \frac{\partial P_{atm}}{\partial x_i} - g\rho_0\frac{\partial \eta}{\partial x_i} - g\int_z^\eta \eta\frac{\partial \rho'}{\partial x_i} dz \tag{2.3}$$

The total pressure gradient is the sum of the gradients of the atmospheric pressure, the sea surface elevation (barotropic pressure gradient) and the density distribution (baroclinic pressure gradient). This decomposition is substituted in the 3D incompressible primitive equations and yields to the ***mass momentum equation***:

$$\frac{\partial u_i}{\partial t} + \frac{\partial (u_i u_j)}{\partial x_j} = -\frac{1}{\rho_0}\frac{\partial P_{atm}}{\partial x_i} - g\frac{\rho(\eta)}{\rho_0}\frac{\partial \eta}{\partial x_i} - \frac{g}{\rho_0}\int_{x_3}^{\eta}\frac{\partial \rho'}{\partial x_i}dx_3 + \frac{\partial}{\partial x_j}\left(\upsilon\frac{\partial u_i}{\partial x_j}\right) - 2\varepsilon_{ijk}\Omega_{ijk} \quad (2.4)$$

where u_i are the velocity vector components in the Cartesian x_i directions, υ is the turbulent friction and p_{atm} is the atmospheric pressure. ρ is the density, ρ' is its anomaly, ρ_0 is the reference density, $\rho(\eta)$ represents the density at the free surface, g is the acceleration of gravity, t is the time, Ω is the Earth's velocity of rotation and ε is the alternate tensor. The ***mass balance equation (continuity)*** is:

$$\frac{\partial u_i}{\partial x_i} = 0 \quad (2.5)$$

The density ρ is calculated as a function of temperature and salinity by the ***equation of state*** [Leendertse and Liu, 1978]:

$$\rho = (5890 + 38T - 0.375T^2 + 3S)/((1779.5 + 11.25T - 0.0745T^2) - (3.8 + 0.01T)S + 0.698(5890 + 38T - 0.375T^2 + 3S)) \quad (2.6)$$

This equation is an approximation for shallow water of the most widely used UNESCO equation [UNESCO, 1981]. The vertical velocity is calculated from the continuity equation by integrating between the bottom and the depth z where u_3 is to be calculated:

$$u_3(x_3) = \frac{\partial}{\partial x_1}\int_{-h}^{x_3} u_1 dx_3 - \frac{\partial}{\partial x_2}\int_{-h}^{x_3} u_2 dx_3 \quad (2.7)$$

The free surface equation is obtained by integrating the ***continuity equation*** over the whole water column:

$$\frac{\partial \eta}{\partial t} = \frac{\partial}{\partial x_1}\int_{-h}^{\eta} u_1 dx_3 - \frac{\partial}{\partial x_2}\int_{-h}^{\eta} u_2 dx_3 \quad (2.8)$$

The model also solves a ***transport equation*** for salinity, water temperature or any other tracer:

$$\frac{\partial \alpha}{\partial t} + u_j\frac{\partial \alpha}{\partial x_j} = \frac{\partial}{\partial x_j}\left(K\frac{\partial \alpha}{\partial x_j}\right) + FP \quad (2.9)$$

where α is the transported property, K is the diffusion coefficient and FP is a possible source or sink term.

2.1.2. Boundary conditions

• Free surface

At the free surface boundary all advective fluxes across the surface are assumed null, i.e. imposing a null J vertical flux:

$$Jflux \mid surface = 0 \quad (2.10)$$

Diffusive flux of momentum is imposed assuming explicitly a wind surface stress, $\overrightarrow{\tau_W}$:

$$\upsilon_3\frac{\partial u_1}{\partial x_3} \mid surface = \overrightarrow{\tau_W}, i = 1,2 \quad (2.11)$$

where υ_3 is the vertical eddy friction. The wind stress is calculated according to a quadratic friction law:

$$\overrightarrow{\tau_W} = C_D \rho_a \overrightarrow{W} |\overrightarrow{W}| \quad (2.12)$$

where *CD* is a drag coefficient that is a function of the wind speed, ρ_a is the air density and $\overrightarrow{W}$ is the wind speed measured 10 m above the sea surface. In this study, the wind stress was not considered. Temperature and salinity advective fluxes are imposed null. Other fluxes of heat and freshwater are introduced as a source (or a sink) term in the transport equation.

• Bottom boundary

At the bottom, the water flux is also assumed to be null and the bottom stress is calculated using a non-slip method with a quadratic law that depends on the near bottom velocity. This condition can be expressed by:

$$\upsilon_3 \frac{\partial u_i}{\partial x_3} |bottom = C_D u_i \sqrt{u_1^2 + u_2^2}, i = 1,2 \quad (2.13)$$

where *CD* is the bottom drag coefficient, which is calculated for flows 2D:

$$C_D = gnH^{-\frac{1}{3}} \quad (2.14)$$

where *g* is the gravity, *n* is the Manning coefficient, *H* is the depth of the water column. For stability reasons, this term is calculated implicitly in the momentum equation of the bottom cell, using a procedure described by Backhaus [1983]. No salinity and temperature fluxes are considered at the bottom.

• Lateral closed boundaries

The closed boundaries of the domain correspond to land. A free slip condition is used to resolve this lateral boundary:

$$\frac{\partial u_1}{\partial x_2} = \frac{\partial u_2}{\partial x_1}, u_i . n_i = 0, i = 1,2 \quad (2.15)$$

Using the finite volume approach, these conditions are implemented specifying zero water fluxes and zero momentum diffusive fluxes for the cell faces in contact with land.

The lateral boundary condition at coastal boundaries is a free slip condition, imposed by specifying a zero normal component of mass and momentum diffusive fluxes at cell faces in contact with land.

• Open boundaries

These boundaries are necessary to confine the domain to the study area. The information imposed here must guarantee that what is happen outside the study area enters in order that the solution inside the domain is not corrupted. Also, waves inside the domain should be allowed to go out. Perfect open boundary condition does not exist, being the most suitable ones those depending on the phenomena to be modelled. At the ocean open boundary the free surface elevation is specified and at the river boundaries the water flow is imposed.

• Moving boundaries

Moving boundaries are closed boundaries whose positions change in time. This arises in domains with intertidal areas where some points can be covered or uncovered depending on the tidal elevation. In this case the uncovered cells must be tracked. The criterion used in MOHID is well described by Martins [2000],

Martins *et al.* [2001] and Leitão [2003] and can be found in the assessment of MOHID-2D in the Ria de Aveiro [Vaz *et al.* 2005a; 2007].

This situation appears in domains with intertidal zones, which are very common in the Sado estuary. In this case the uncovered cells must be tracked and with this purpose a criteria based on Figure 6 is used. *HMIN* is the depth bellow which the cell is considered uncovered. In this case a thin volume of water above the uncovered cell is conserved. The cells of position *i*, *j* are considered uncovered when one of the two following situations is true:

$$H_{ij} < HMIN \wedge \eta_{ij-1} < -h_{ij} + HMIN \quad (2.16)$$

$$H_{ij-1} < HMIN \wedge \eta_{ij} < -h_{ij-1} + HMIN \quad (2.17)$$

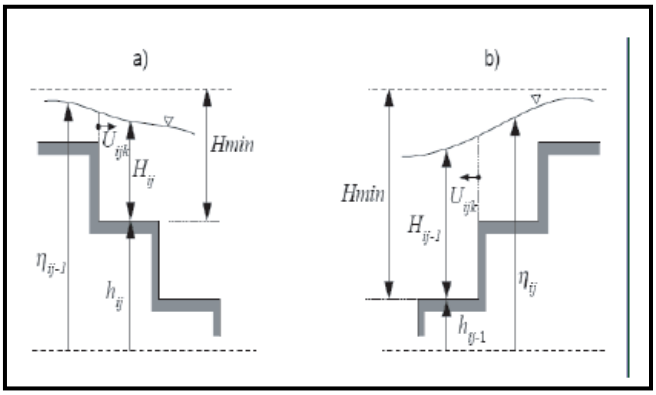

Figure 5 - Conditions for a point to be considered uncovered (moving boundaries) (Leitão;2003).

The second condition of (2.16) assures that the cell is not being covered by the tidal wave propagating from left to right and the second condition of (2.17) assures that the cell is not being covered by the tidal wave propagating from right to left. The noise formed by the abrupt change in velocity at the dry cells is controlled with a careful choice of *HMIN* (in this case *HMIN* = 0.10 m) [Leendertse and Liu, 1978].

Bathymetry is an important factor affecting shallow waters, once it controls the current spatial variability and direction, revealing and assuring the realism of the numerical model. The used bathymetry should be satisfactorily refined to resolve the geometry and depth variations. For this study a grid of 128×158 points was used, obtained from depth sounding data made by I***nstituto Hidrográfico*** (Marateca and Carrasqueira 1968, exterior zone 1977, mouth and inner estuary until Setenave 1980).

2.1.3.Surface heat fluxes parameterizations

Estuarine regions are highly subject to air-water interactive processes. The relative shallowness of these areas results in a significant temporal variability (daily, monthly or seasonal) which may exceed that of open oceanic waters. Furthermore, the relative importance of the individual terms of the heat budget equation could be quite different. The water-air heat changes are influenced by five distinct processes: solar shortwave radiation, atmospheric long wave radiation, water long wave radiation, sensible and latent heat flux. In MOHID, the total heat surface flux is obtained by adding the last three processes referred above. The solar

end atmospheric radiation penetrating in the water column is converted in heat. The radiation entering the water column is parameterized as an exponential function of depth by the law proposed by Kraus [1972]:

$$\boldsymbol{I(z) = F_{sol}\left(I_1 e^{-z/\lambda_1} + I_2 e^{-z/\lambda_2}\right), I_2 = 1 - I_1} \quad (2.19)$$

Indexes 1 and 2 refer to the long and shortwave radiation components, respectively. *z* is positive downward, being *z* = 0 the sea surface. Values of I_1, λ_1 and λ_2 where published by Paulson and Simpson [1977] according to the classification found in Jerlov [1968]. These coefficients depend on the type of water of the study area. In order to quantify the incoming solar radiation in the water surface, MOHID uses the formulation found in Brock [1981] which depends on the sun height, atmospheric absorption and albedo. The formulation is given by:

$$\boldsymbol{R_S = (1 - albedo) \times QS_0 \times AT \times neb} \quad (2.20)$$

where R_s is the incoming solar radiation (Wm^{-2}), QS_0 is the Solar Constant (Wm^{-2}), *AT* is the atmospheric transference, *neb* is the nebulosity (% of cloud cover). QS_0 varies with the latitude, time of the year and day hour. The net longwave radiation R_a (Wm^{-2}) is calculated using [Swinbank, 1963]:

$$\boldsymbol{R_a = 0.937 \times 10^{-5} \sigma (273.15 + T_a)^6 (1 + 0.17 neb^2)(1 - R_e)} \quad (2.21)$$

where σ is the Stefan-Boltzman constant (5.6697×10^{-8} $Wm^{-2}K^{-4}$) and *Re* is the radiation reflected by the sea surface (%). The infrared radiation R_{br} (Wm^{-2}) is calculated applying the Stefan-Boltzman law:

$$\boldsymbol{R_{br} = \varepsilon \times \sigma \times (273.15 + T_w)^4} \quad (2.22)$$

here ε is the water emissivity (≈0.97) and T_w is the water temperature (K). The latent H_L and sensible *Hs* heat fluxes (in (Wm^{-2})) are calculated using the Dalton and Bowen laws, respectively (adapted from Chapra [1997]):

$$\boldsymbol{H_L = (19.0 + 0.95 U_w^2) \times \left(e_{s,w} - r_h \times e_{s,a}\right)} \quad (2.23)$$

$$\boldsymbol{H_s = C_b \times (19.0 + 0.95 \times U_w^2) \times (T_w - T_a)} \quad (2.24)$$

where U_w is the wind speed (ms^{-1}), $e_{s,w}$ is the saturated water pressure (mmHg), r_h is the relative humidity (values between 0 and 1), $e_{s,a}$ is the air saturation pressure (mmHg), C_b is the Bowen coefficient (≈0.47 $mmHGK^{-1}$), T_w and T_a is the water and air temperature (K). The latent heat flux is directly related to the pressure vapour deficit and the sensible heat is related to the water-air temperature difference.

2.2. Model Validation – SADO Estuary case

In this study is used a configuration of Mohid previously implemented for the Sado Estuary. Nevertheless in the following a brief description of some results regarding the model's calibration and validation will be given. In order to calibrate the model a comparison between model output and available *in situ* data is needed to prove the model efficiency. The measurements used to perform the validation have to be independent from the data set used for calibration.

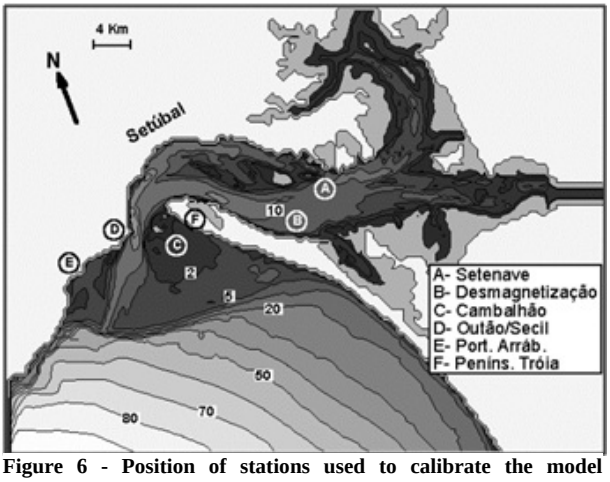

Figure 6 - Position of stations used to calibrate the model (source: Ribeiro and Neves (1982).

The hydrodynamic model was calibrated using elevation sea level data from six tidal stations and velocity data from 6 currentmeter stations (A,B,C,D,E and F) placed in the estuary interior Ribeiro and Neves [1982] (Figure 7). The studies developed by Ambar *et al.* [1980], Ribeiro and Neves [1982], Neves [1985a;b] have provided information to generally characterize the physical conditions of Sado estuary and supplied data for the calibration and validation of the hydrodynamic and transport models.

In Figure 8a), are shown typical current directions at the inlet and in several locations inside the estuary [Ribeiro and Neves 1982]. These results show high concurrence with the instant velocity fields obtained with the model to the same tidal conditions. The salinity fields in flood and ebb moments (Figures 8b) and c)) show the same conditions of agreement and the TS-diagrams presented by Wollast *et al* [1978] showed two dilution lines, one for the principal estuary and other for the Álcacer channel as expected. In all the stations the results show good concordance. Figure 8d) shows the comparison between a time series of sea level from a station situated near Setenave and the results from the model. Figure 8e) depicts the comparison of the current velocity for the demagnetization station situated in the south of the channel. Although the existence of a high variability and taking into account the small time interval analyzed, the numerical results are acceptable once they are in the same order of magnitude and the broadcast of the inversion of tide moments are correct. The downstream estuary limit is considered to be the red line showed in Figure 8f) and stations coordinates in Table 4 [Martins *et. al*; 2001].

The meteorological data used in the model simulations were extracted from Guía station (source: http://maretec.mohid.com/).

a)

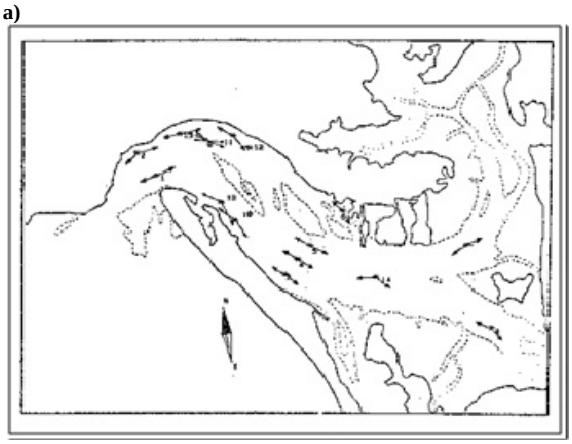

(Source: Ribeiro and Neves, 1982)

b)

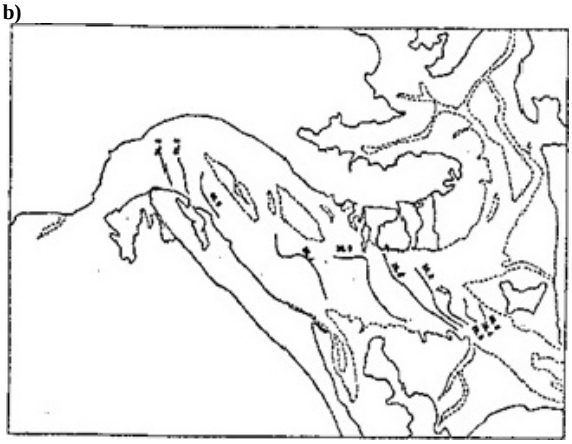

(Source: Ribeiro and Neves, 1982)

c)

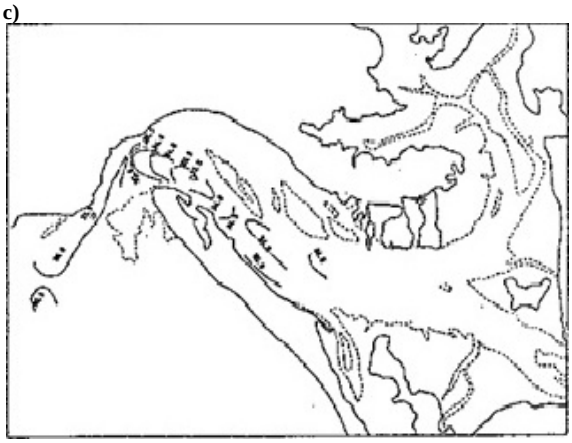

(Source: Ribeiro and Neves, 1982)

d)

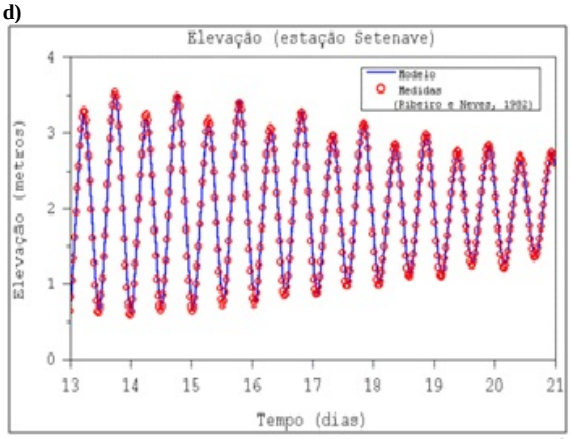

(Source: http://www.inag.pt/)

e)

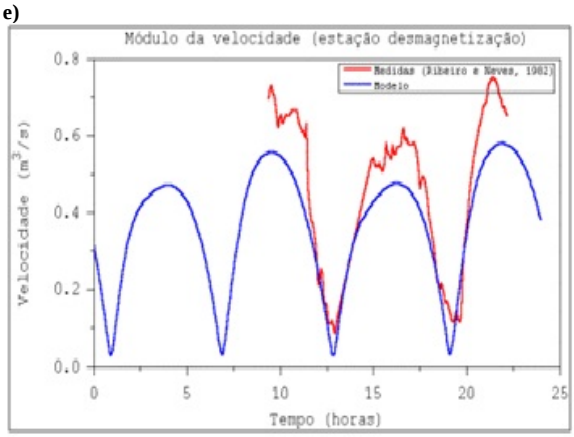

(Source: http://www.inag.pt/)

f)

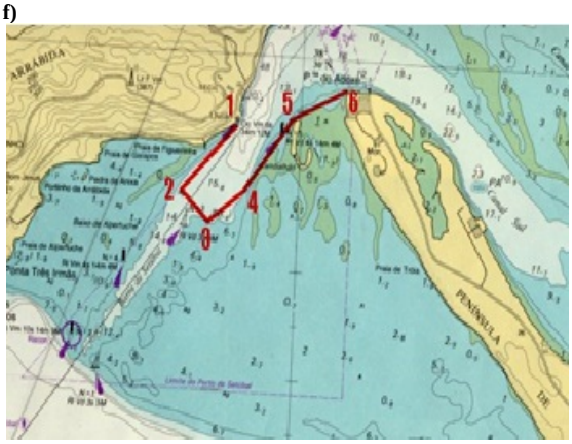

(Source: http://www.inag.pt/)

Figure 7 - a) Typical current directions of inlet and outlet b) Isoline salinities in the beginning of flood for July month 1979, values of 32 near the mouth and 28 at entrance of the Alcácer channel c) Typical current directions of inlet and d) Calibration of the hydrodynamical model: comparison of sea levels for Setenave station e) Hydrodynamic model calibration, current velocity comparison for the demagnetization station f) Map showing the estuary downstream limit: red line with station 1–6.

Table 4 - Station coordinates delimitating the dowtream limit of Sado estuary (Source: http://www.inag.pt/estuarios/)

Estação	Latitude (N)	Longitude (W)
1	38º29’18’’	8º56’00’’
2	38º28’36’’	8º56’54’’
3	38º28’24’’	8º56’24’’
4	38º28’45’’	8º55’48’’
5	38º29’24’’	8º55’06’’
6	38º29’42’’	8º54’24’’

III. RESULTS and DISCUSSION

This work is divided in two parts: hydrodynamics and fecal coliform dispersion. In the first, sea surface height, current velocity, water temperature and salinity spatial patterns will be studied, in order to evaluate their modifications due to changes in tidal and river inflow forcing, and bottom friction. In the second part tidal advection effects on different local sewage discharge values will be analysed, observing the fecal coliforms dispersion in the estuary.

3.1. General description

In order to study the salinity, water temperature, velocity, and sea surface height variability, induced by different tidal and river inflow(2, 50 and 200 m^3/s), as well as evaluate the changes induced by bottom friction modifications (Manning values of 0.0025 and 0.0075$m^{1/3e}s^{-1}$), several scenarios were defined. Spring and neap tides and different tidal cycle moments (high, low, flood and ebb tide) where chosen. Figure 9 shows the location of the stations where simulated values were extracted, and also the discharge points used for the model simulations in the Sado Estuary. The location of each stations was specifically chosen in order to capture the different behaviour of the various variable: station 1 just after the mouth, station 2 at the mouth, station 3 just after the mouth in the inner estuary, station 4 in the middle estuary and stations 5 and 6 in the upper and lower channels of the estuary.

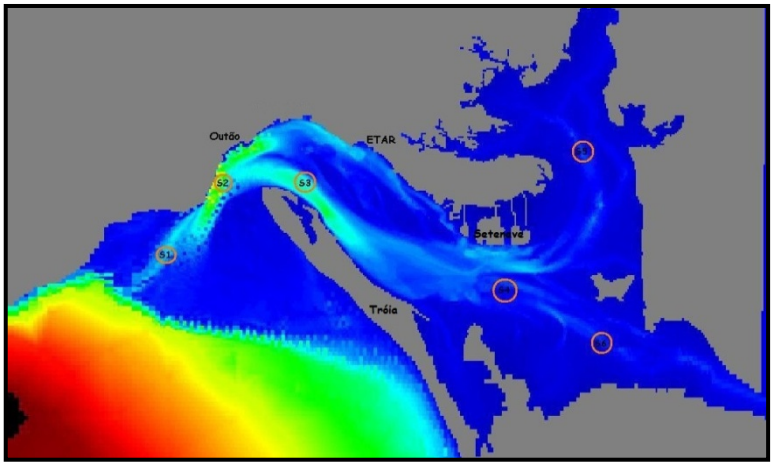

Figure 8 - Stations location in Sado estuary, where data from the model where extracted for comparison, and reference points Outão and ETAR (discharge sewage points used in the model), Setenave and Tróia peninsula.

The coordinate values for discharge sewage points used in model simulations, station location in Sado estuary and finally the model run periods are showed in Tables 5, 6 and 7. The whole period under analysis comprised 3 months, starting on the 11th January and ending at 11th April 2009. In terms of bottom friction and river inflow table 5 shows the values used for each simulation.

Table 5 - Discharge point in Sado Estuary simulation

Discharge points	i	j	x	y	z
Outão	133	87	132024,6	171832,5	0
ETAR	127	157	137268,6	171368,4	0

Table 6 - Stations coordinates i, j, x, y e z.

Stations	i	j	x	y
St 1	71	41	128452,3	167196,5
St 2	112	72	130892,9	170259,2
St 3	112	118	134370,4	170247
St 4	51	231	142815,4	165685
St 5	130	275	146095,5	171599
St 6	29	186	146924,6	163401

Table 7 – Run periods considered for all simulations

Runs	Period
Run 1 Spin up	11/01 – 13/01
Run 2	13/01 - 20/01
Run 3	20/01 - 28/01
Run 4	28/01 - 04/02
Run 5	04/02 - 11/02
Run 6	11/02 - 21/02
Run 7	21/02 - 11/03
Run 8	11/03 - 11/04
Run 9	11/02 - 11/04

3.2. Hydrodynamics and Hydrology

In this section the river runoff and bottom friction effects will be studied in order to evaluate the hydrodynamic/hydrographic features of the estuary.

"The Sado River flows into the estuary through the Alcácer channel, it is characterized by particularly high flow rates during very wet winters, when the discharge can reach 250 m^3/s, while in dry season flow rates of 1-3m^3/s are usually recorded" [Martins *et al.*, 1998]. Considering this statement two values of river inflow (***Q***) were chosen for model simulations: 200 m^3/s and 2 m^3/s. For the bottom friction effect evaluation, the Manning values (directly related to friction) used in the simulations were 0.0025 $m^{(1/3)}s^{-1}$ and 0.0075 $m^{(1/3)}s^{-1}$. The *spin up* period was of two days in order to stabilize the model. To analyse the river runoff effect, simulations 1 and 2 or 3 and 4 can be compared. For the bottom friction effect analysis, simulations 1 and 3 or 2 and 4 can be compared (see Figure 9).

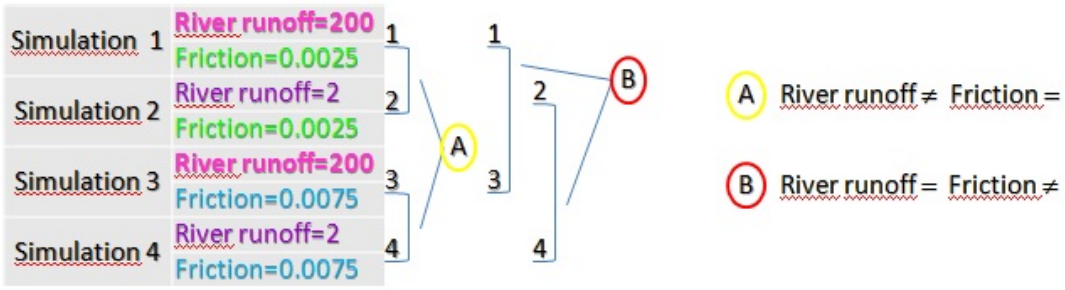

Figure 9 - Manning and river inflow values used in the model simulations. A encloses simulations with different river inflow values (2 or 200m^3s^{-1}) and same Manning value (0.0025/0.0075 $m^{(1/3)}s^{-1}$), B encloses simulations with river inflow equal (2/200m^3s^{-1}) and different Manning value (0.0025 or 0.0075 $m^{(1/3)}s^{-1}$).

3.2.1.Bottom friction effect

The bottom friction effect over the propagation of the tidal wave will be analyzed using Manning values of 0.0025 $m^{(1/3)}s^{-1}$ and 0.0075 $m^{(1/3)}s^{-1}$ for a river inflow of 200 m^3s^{-1}. Simulations 1 and 3 were chosen for comparison (see Figure 9).

3.2.1.1. Current velocity horizontal structure

In order to describe the horizontal structure of the current velocity, simulations 1 and 3 were compared for high tide moments, and river inflow of 200 m^3s^{-1}, using Manning values of 0.0025 $m^{(1/3)}s^{-1}$ (Figures 10a) and b) and 0.0075 $m^{(1/3)}s^{-1}$ (Figures 10c) and d).

In general, it is clearly visible that the higher velocity values (≈0.638-0.850 ms^{-1}) are found near the estuary mouth (Figures 10 a) and c)), and the smaller along the estuary (in the inner region), presenting values of ≈0.2 ms^{-1} and in particularly areas, like near the city shoreline (only seen for Figure 10 a)), values of 0.425 ms^{-1}.

For the Manning value of 0.0075 $m^{(1/3)}s^{-1}$ (Figure 10c) and d) velocity shows lower values (<≈0.2ms^{-1}) than for the Manning value of 0.0025$m^{(1/3)}s^{-1}$ (Figures 10a) and b), as it was expected, since bottom friction enlarges its importance when the tidal wave enters the estuary, where the water column is shallower. In other words, for higher values of bottom friction the velocity and sea surface height suffer higher transformations inside the estuary (changes in amplitude and phase). As for spring (Figures 10a) and c) and neap tides (Figures 10b) and d), the highest velocity values were found for spring tide as expected, and in neaps tide the velocities are considerably smaller (≈0.4ms^{-1}).

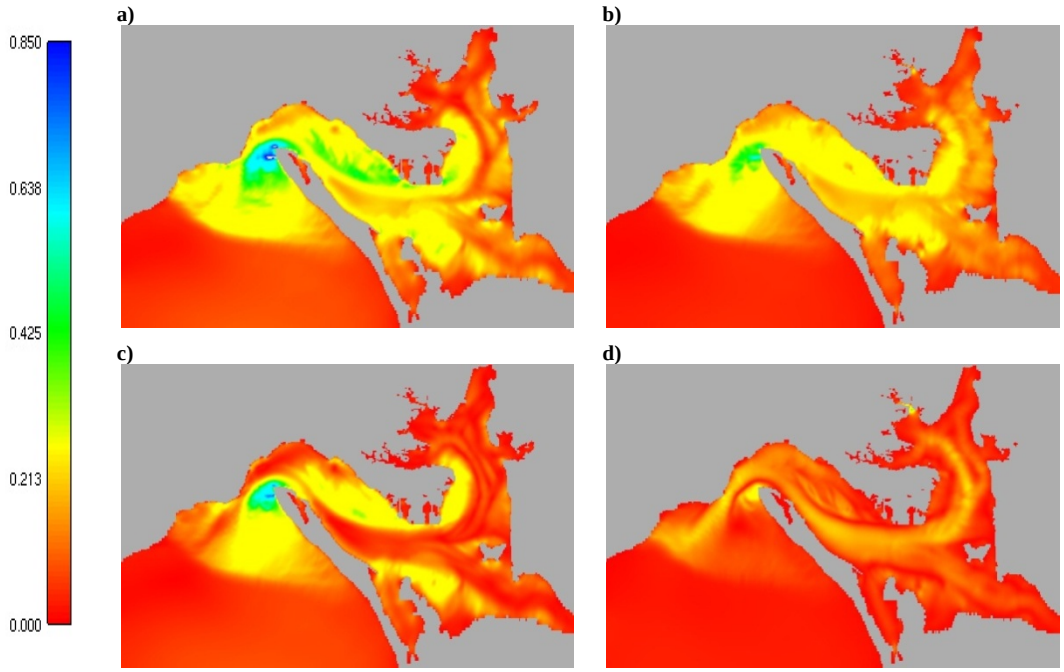

Figure 10 –Current intensity fields, all figures for a river inflow=200 m^3s^{-1} : a) Simulation 1, high tide, spring tide b) Simulation 1, high tide, neap tide. c) Simulation 3, high tide, spring tide. d) Simulation 3, high tide, neap tide. Maximum values found at the estuary mouth for a) and c) ≈0.638-0.850 m/s for b) ≈0.425-0.638 m/s and for d) the lowest values ≈0.213 m/s.

To better evaluate the current velocity horizontal structure, time series of velocity and sea surface height are plotted in Figure 11. Station 1 (right after the mouth) and station 4 (in the middle estuary) were chosen for data extraction and comparison (see Figure 9). Current velocity and sea surface height range for both simulations and stations are depicted in Table 9. Moreover, differences between stations and simulations maximum and minimum velocity and sea surface height values can be observed, as well as tidal amplitude. The results show that the current velocity at station 1 is higher (reaching ≈1.2 ms^{-1}) than the velocity found for station 4 (only reaching ≈0.8 ms^{-1}) (see Figure 11).

A compilation of the most important results is presented in Table 9. For the sea surface height, the results show to be higher in station 4 (reaching maximums of 3.95 m for simulation 1 and 3.91 m for simulation 3) than in station 1 (reaching values of 3.72 m for simulation 1 and 3.71 m for simulation 3). This is an expected result since station 4 is in the middle estuary and the tidal amplitude is amplified at this location (see Table 9). The amplitude values confirm to be higher in station 4, with 3.80 m for simulation 1 and 3.73 m for simulation 3, than in station 1 where values of 3.34 m for simulation 1 and 3.32 m for simulation 3 can be found (see Table 9). The current velocity values show higher values in station 1 (reaching 1.16 ms^{-1} for simulation 1 and 1.13 ms^{-1} for simulation 3) than in station 4 (only reaching 0.81 ms^{-1} for simulation 1 and 0.76 ms^{-1} for simulation 3). The values that are shown here are in agreement with the ones presented by Moreira [1987] (see Annex 1).

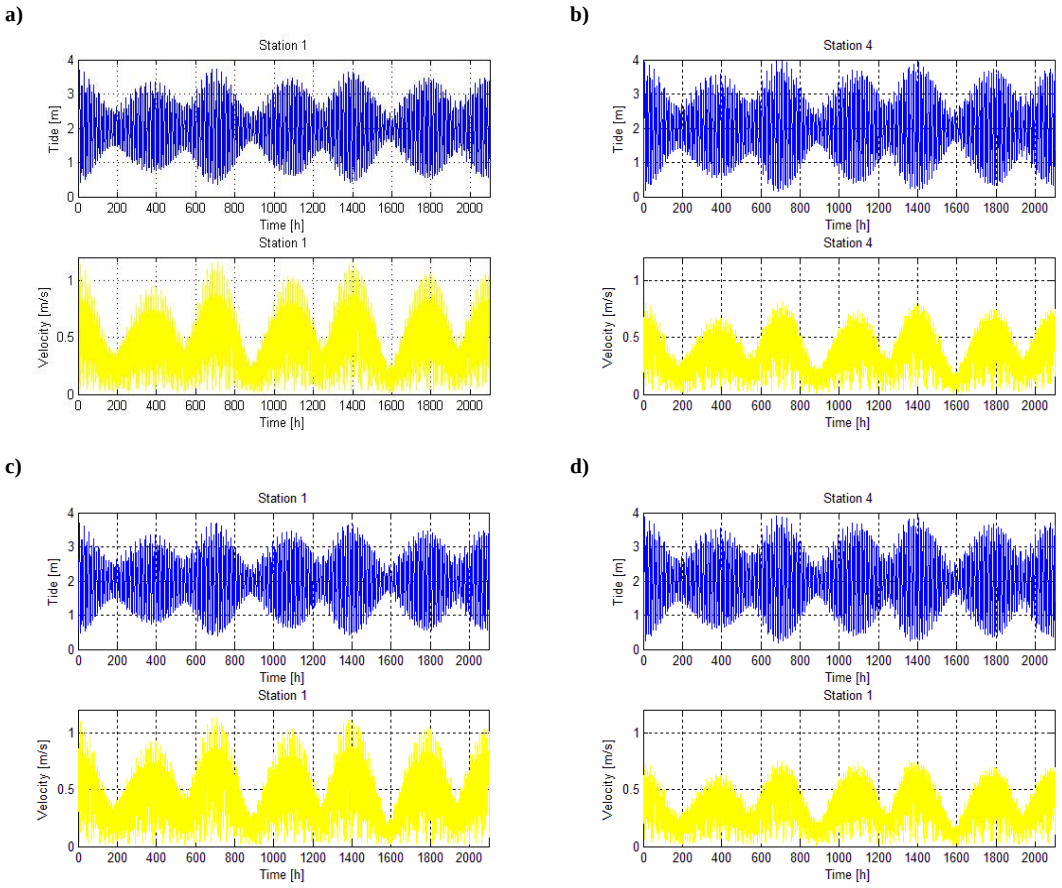

Figure 11 –Temporal series for velocity and sea surface height with river inflow=200 m^3s^{-1}, for: a) Station 1, Simulation 1. b) Station 4, Simulation 1. c) Station 1, Simulation 3. d) Station 4, Simulation 3. Simulation 1 - 0.0025 $m^{(1/3)}s^{-1}$, Simulation 3 - 0.0075 $m^{(1/3)}s^{-1}$

Table 8 - Current velocity and sea surface height range according to simulation 1 and 3, differences between stations and simulations, and tidal amplitude.

		St 1		St 4		Differences between stations	Differences between simulations		
Sim 1	Velocity	min	0.02	min	0.01	0.01	Min	max	St 1
		max	1.16	max	0.81	0.35	0.00	0.03	
Sim3		min	0.02	min	0.01	0.01	Min	max	St 4
		max	1.13	max	0.76	0.37	0.00	0.05	
Sim 1	Sea surface height	min	0.38	min	0.15	0.23			
		max	3.72	max	3.95	-0.23			
Sim3		min	0.39	min	0.18	0.21			
		max	3.71	max	3.91	-0.20			
Sim 1	Tidal amplitude	3.34		3.80					
Sim 3		3.32		3.73					

Comparing the results for both simulations (Figure 11 and Table 9), it is possible to conclude that when the Manning value (bottom friction) is 0.0075 $m^{(1/3)}s^{-1}$ both velocity and tidal amplitude reveal to be lower than for the Manning value of 0.0025 $m^{(1/3)}s^{-1}$. This pattern is explained by the delay in tidal propagation when friction increases.

Maldonado Soto [2004] also concluded that when friction is lower, the tidal amplitude is higher, and that lower friction induces lower loss of tidal energy.

3.2.1.2. Spectral Analysis

Spectral density plots are used to determine the power spectrum and to find periodic phenomena. Data were worked on Matlab software, routines were made in order to determine spectral density. Time series used comprised the whole two month of simulation. Before performing the spectral analysis, the time series trend and mean were removed (see Annex 3). Spectral energy density plots of sea surface height and current velocity are shown in Figure 13, for simulations 1 (Manning value: 0.0025 $m^{(1/3)}s^{-1}$) and 3 (Manning value: 0.0075 $m^{(1/3)}s^{-1}$) and for stations 1 (right after the mouth) and 4 (in the middle estuary), with river inflow 200 m^3/s. Through the number of cycles per day (cpd) it is possible to identify some periodicities and connect them to the tidal components (1cpd – M_2 and S_2, 2cpd – O_1 and K_1, 4cpd – M_4, 6cpd – M_6, etc).
For sea surface heights, the most energetic peaks, for both stations (Figures 13 a) b) e) f)), are detected for the semidiurnal and diurnal frequencies, with higher energy associated to the first one. For the fourth and six-diurnal frequencies, inside the estuary (station 4), the energetic peaks are twice higher (high spectral energy) than near the mouth (station 1), revealing its amplification as the tidal wave enters the estuary. For the velocity plots the frequencies that show higher energy are the fourth and six-diurnal, followed by semidiurnal and diurnal. The values reveal to be slightly higher near the mouth (station 1) than in the inner estuary (station 4). They fade towards the inner estuary for the Manning value 0.0025 $m^{(1/3)}s^{-1}$(simulation 1, Figures 13c) and d)), while they are amplified for the value 0.0075 $m^{(1/3)}s^{-1}$ (simulation 3, Figures 13g) and h)).

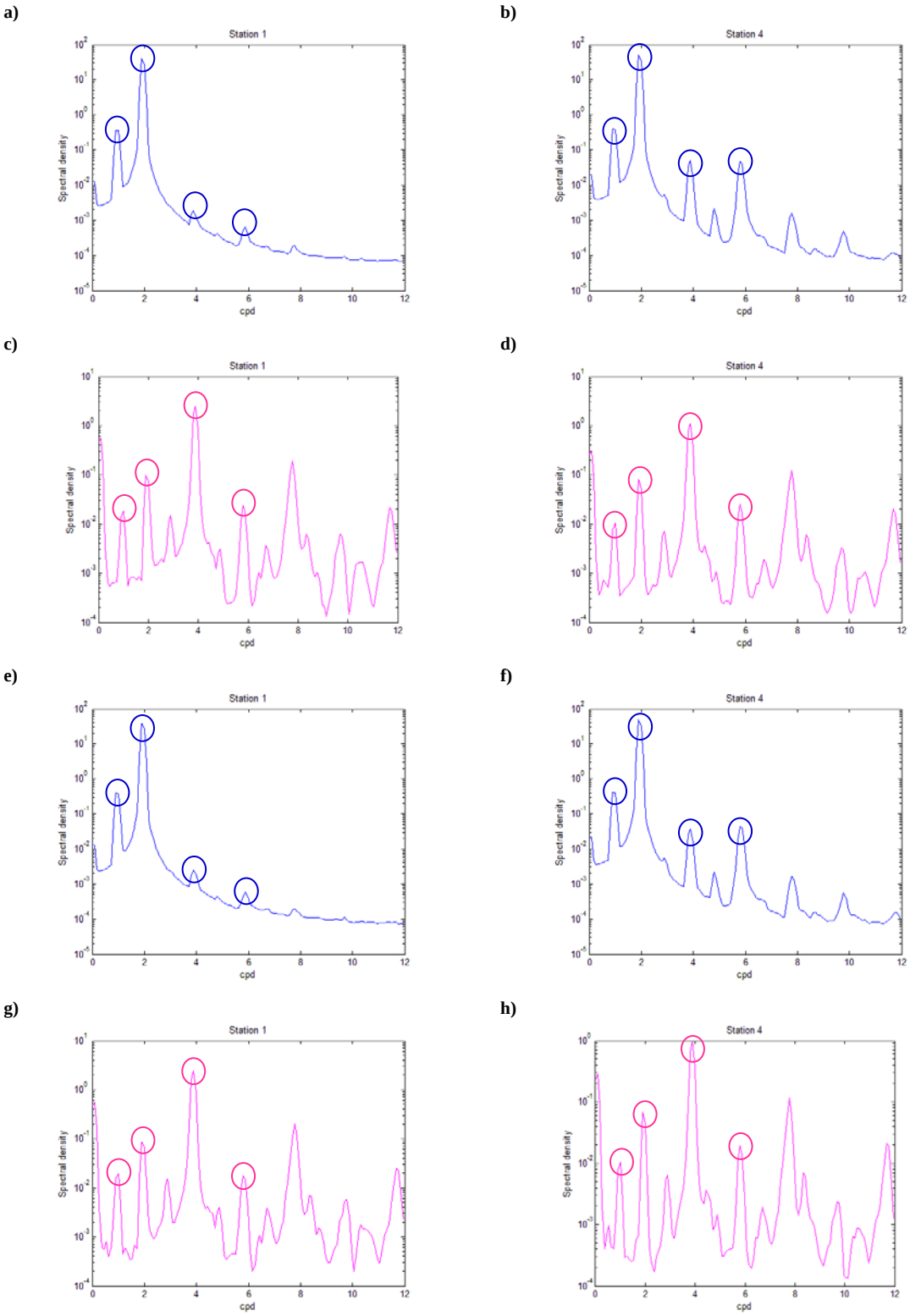

Figure 12 – Spectral density plots of sea surface height (blue) and velocity (magenta) for simulations 1 and 3 and for stations 1 and 4, for river inflow 200 m^3/s: a) Station 1, Simulation 1, sea surface height b) Station 4, Simulation 1, sea surface height c) Station 1, Simulation 1, velocity d) Station 4, Simulation 1, velocity e) Station 1, Simulation 3, sea surface height f) Station 4, Simulation 3, sea surface height g) Station 1, Simulation 3, velocity h) Station 4, Simulation 3, velocity. Cpd – cycles per day, simulation 1 – Manning value: 0.0025 $m^{(1/3)}s^{-1}$), simulation 3 – Manning value: 0.0025 $m^{(1/3)}s^{-1}$.

3.2.1.3. Harmonic Analysis

The relative importance of the tidal constituents along the Sado estuary can be evaluated through the application of the classical harmonic analysis package (Pawlowicz *et al*., 2002) to the model data. The six major tidal constituents are: O_1-25,82h (principal Lunar, diurnal), K_1-23.93h (principal solar, diurnal), M_2-12.42h (principal lunar, semi-diurnal), S_2-12h (principal solar, semi-diurnal), M_4 and M_6 (shallow water terms, descendant of M_2 ($2\times M_2$ and $3\times M_2$). The last constituents quantify the importance of bottom friction. Their amplitude and phase results are plotted in Figure 13 for stations 1, 2, 3 and 4 (see in Annex 2 Tables 13 e 14 for more information about other tidal constituents).

For this assessment, two bottom friction values (Manning values of 0.0025 $m^{(1/3)}s^{-1}$ and 0.0075 $m^{(1/3)}s^{-1}$) were chosen in order to simulate the tidal propagation inside the Sado estuary.

Through the analysis of Figures 13a) and b), representing the amplitude values, it can be observed that the major tidal constituents are M_2 (0.5 m (Sts. 1 and 4) and 1 m (Sts. 2 and 3) for Simulation 1 and ≈1 m for Simulation 3 for all stations) and S_2 (0.3 m (Sts. 1 and 4) and 0.5 m (Sts. 2 and 3) for Simulation 1 and ≈0.4 for Simulation 3 for all stations). All the other tidal constituents show amplitude values <0.1 m, for both Manning values (0.0025 $m^{(1/3)}s^{-1}$ and 0.0075 $m^{(1/3)}s^{-1}$), revealing that the semi-diurnal components are dominant. These results are in agreement with Martins *et al.* [2001] that found similar values for M_2 (0.98 m) and S_2 (0.35 m).

For the phase values, S_2 followed by M_2 show the highest values, so these will be the components with higher delay. When compared for simulations 1 and 3 it's possible to observe them fading with the amplification of Manning value while O_1 and K_1 are enhanced, so these last will have lower delay than the first components. For shallow water phase components, M_6 showed to be diminished with amplification of Manning value and the M_4 component behaviour showed to increase upstream, for low Manning value, showing low delay in the wave reproduction.

When the estuary becomes shallower, the bottom friction increases its importance over the propagation of the tidal wave, due to the lower depth and topography influence, generating distortions in the tidal wave principal constituents and oscillations in sea surface heights [Gallo, 2004].

These results are consistent with the ones obtained using the Spectral analysis (see previous section (3.2.1.2.)).

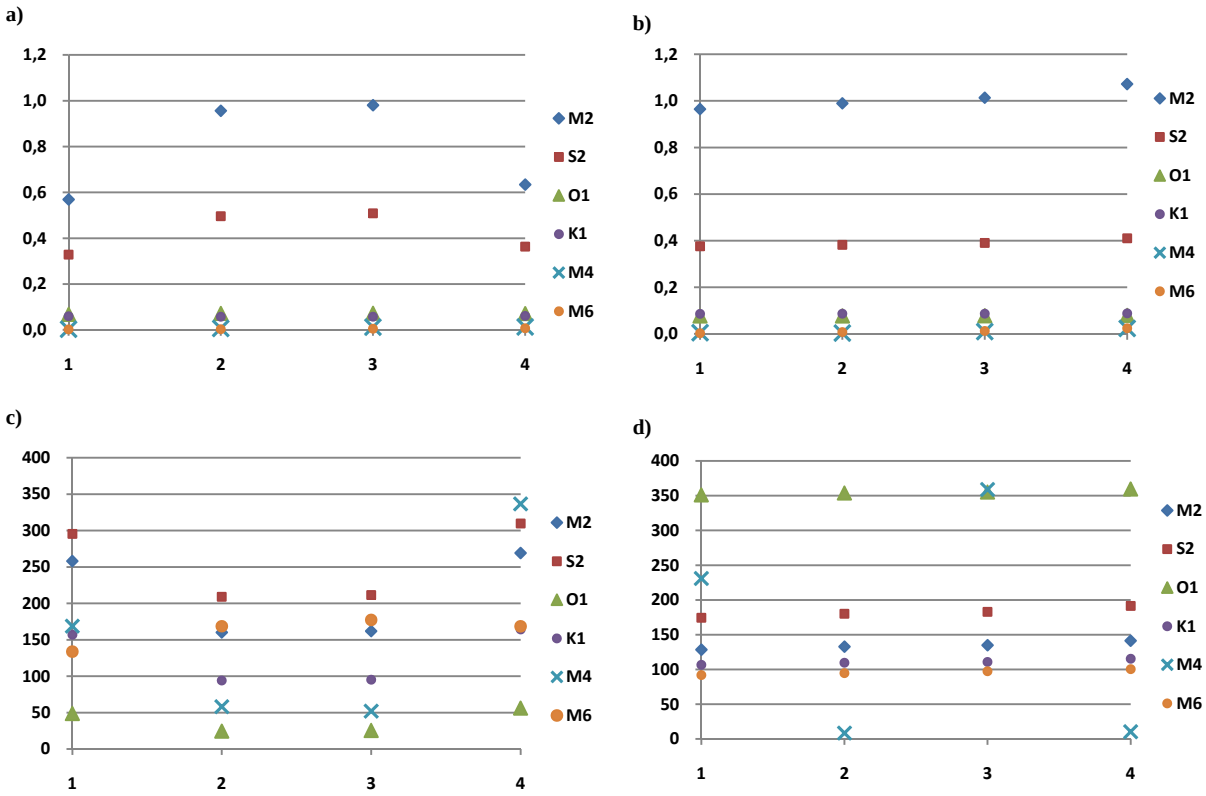

Figure 13 - Amplitude and phase values for stations 1, 2, 3 and 4 for the same river inflow (200 m^3s^{-1}) and different Manning values of 0.0025 $m^{(1/3)}s^{-1}$ (simulation 1) and 0.0075 $m^{(1/3)}s^{-1}$ (simulation 3): a) Amplitude, Manning=0.0025 b) Amplitude, Manning=0.0075
c) Phase, Manning=0.0025 d) Phase, Manning=0.0075.

Table 9 – Amplitude a) and phase values b) for both simulation 1 (0.0025 $m^{(1/3)}s^{-1}$) and 3 (0.0025 $m^{(1/3)}$ s^{-1}) for the tidal constituents M_2, S_2, O_1, K_1, M_4 and M_6.

a)

Tidal constituents	Manning value ($m^{(1/3)}s^{-1}$)	Amplitude (m)
M_2	0.0025	0.5-1
	0.0075	≈1
S_2	0.0025	0.3-0.5
	0.0075	≈0.4
O_1	0.0025 and 0.0075	< 0.1
K_1		
M_4		
M_6		

b)

Tidal constituents	Manning value ($m^{(1/3)}s^{-1}$)	Phase (°)
M_2	0.0025	160-270
	0.0075	125-141
S_2	0.0025	200-310
	0.0075	< 200
O_1	0.0025	< 50
	0.0075	>300
K_1	0.0025	94-165
	0.0075	105-165
M_4	0.0025	St1 170, St2 e 3 50-60, St4 >300
	0.0075	St1 230, St2 e 4 <10, St3 >350
M_6	0.0025	120 - 180
	0.0075	< 100

The Form Number values calculated for river inflow 50 m^3/s (table 11), show that Sado estuary tide confirms to be semi-diurnal (0<Nf<0.25).

Table 10 - Form Number (Nf) values calculated for river inflow=50 m^3/s, for stations 1, 2, 3, 4, 5 and 6.

Station	Nf
1	0.089
2	0.087
3	0.085
4	0.082
5	0.080
6	0.081

3.2.2.River runoff effect

In order to evaluate the river runoff effect on the estuary hydrography, river inflow values of 200 m^3s^{-1}, 50 m^3s^{-1} and 2 m^3s^{-1} were used to represent extreme and mean values of river inflow [Martins *et al.*, 1998]. The Manning value used in these simulations to compute bottom friction was 0.0025 $m^{(1/3)}s^{-1}$.

3.2.2.1. Salinity horizontal structure

In order to describe the salinity horizontal structure, model results for river inflow values of 200 m^3s^{-1}, 50 m^3s^{-1} and 2 m^3s^{-1} were compared for high (Figure 14), ebb (Figure 15), low (Figure 16) and flood (Figure 17) tide moments, using a fix Manning value of 0.0025 $m^{(1/3)}s^{-1}$.

The salinity ranges from fluvial (0 psu) to oceanic typical values (35-37 psu) depending on the freshwater inflow. Observing the salinity horizontal structure, for high tide moments, with river inflow=200 m^3s^{-1} (Figure 14a) and b) and 50 m^3s^{-1} (Figures 14c) and d), in spring (Figures 14a) and c) and neap tides (Figures 14b) and d), it is visible the influence of the freshwater inflow in the salinity patterns found inside the estuary. The freshwater inflow (dark to cyan blue ≈0-9 psu) extends from south channel (where it enters the estuary) until the north channel for Q=200 m^3s^{-1} influencing, in terms of salinity, a large estuary area, covering the two channels. A mixture zone (cyan blue to orange ≈9-30 psu) can be observed in the middle estuary, being this zone moved easterly in spring tide and westerly in neap tide. For Q=50 m^3s^{-1} the entrance of freshwater is diminished reaching only a few kilometres, neither the middle estuary nor the north channel (presenting the north channel values slightly higher than for Q=200 m^3s^{-1} ≈9-18 psu). The mixture area intensifies and covers a higher area than for Q=200 m^3s^{-1} reaching upstream the estuary, more intense for spring tide (Figure 14c), but also observed for neap tide (Figure 14d).

Generally in the Alcácer channel for Q=200 m^3s^{-1} e Q=50 m^3s^{-1}, values of 0 psu are detect reaching a maximum of 6.3 psu (station 6). This result is expected, once is this channel that assures the river freshwater entrance in the estuary. In the north channel, salinity values are slightly higher 2.3-16.8 psu (station 5). For the area that conjoins both channels 5.3-36 psu values are observed (station 4), revealing higher influence of oceanic waters, but still showing low salinity values typical of a clearly mixture area. In the middle estuary salinity values can reach 36 psu but still low values (10.9 psu) can be found, revealing a well defined mixture area. At the mouth (station 2), higher values can be found (16.4-36 psu) revealing higher influence of oceanic waters. As for the area just after the mouth (station 1) the results 25.8-36 psu reveal the influence of the mixture layer that can reach such area in the ebb tide (see Table 12 for values).

Resuming, the river inflow extends its influence further downstream for the simulations with a river inflow of 200 m^3s^{-1} than for the case of river inflow 50 m^3s^{-1}. According to these results it is possible to define three areas in the estuary: one with higher river inflow influence located at the south channel (Alcácer) - for a higher river inflow (200 m^3s^{-1}) it is extended to the north channel; second area located near the mouth where oceanic waters influence prevail; and between these two areas a transition area is evident, with strong horizontal salinity gradients defined as a mixture area.

For low values of river inflow (2 m^3s^{-1}) (Figures 14e) and f) – high tide) differences in the salinity spatial structure for the spring and neap tide are not quite visible, possibly because the mixture with the oceanic waters occurs further upstream, at the entrance of the river in the estuary (south channel), where salinity values of ≈33 psu can be seen, and mixed oceanic water (33-36psu) occupy the rest of the estuary area. River

inflow of 2 m^3s^{-1} is a very small value, turning the influence of oceanic waters the main cause modulating the salinity spatial structure of the entire estuary.

Table 11 - Minimum, maximum and average salinity values (psu) for river inflow 200 m^3s^{-1} in stations 1-6.

Salinity	St 1	St 2	St 3	St 4	St 5	St 6
Minimum observed	25.8	16.4	10.9	5.3	2.3	0.0
Maximim observed	36.0	36.0	36.0	36.0	16.8	6.3
Average	35.0	33.9	30.9	15.2	7.1	0.7

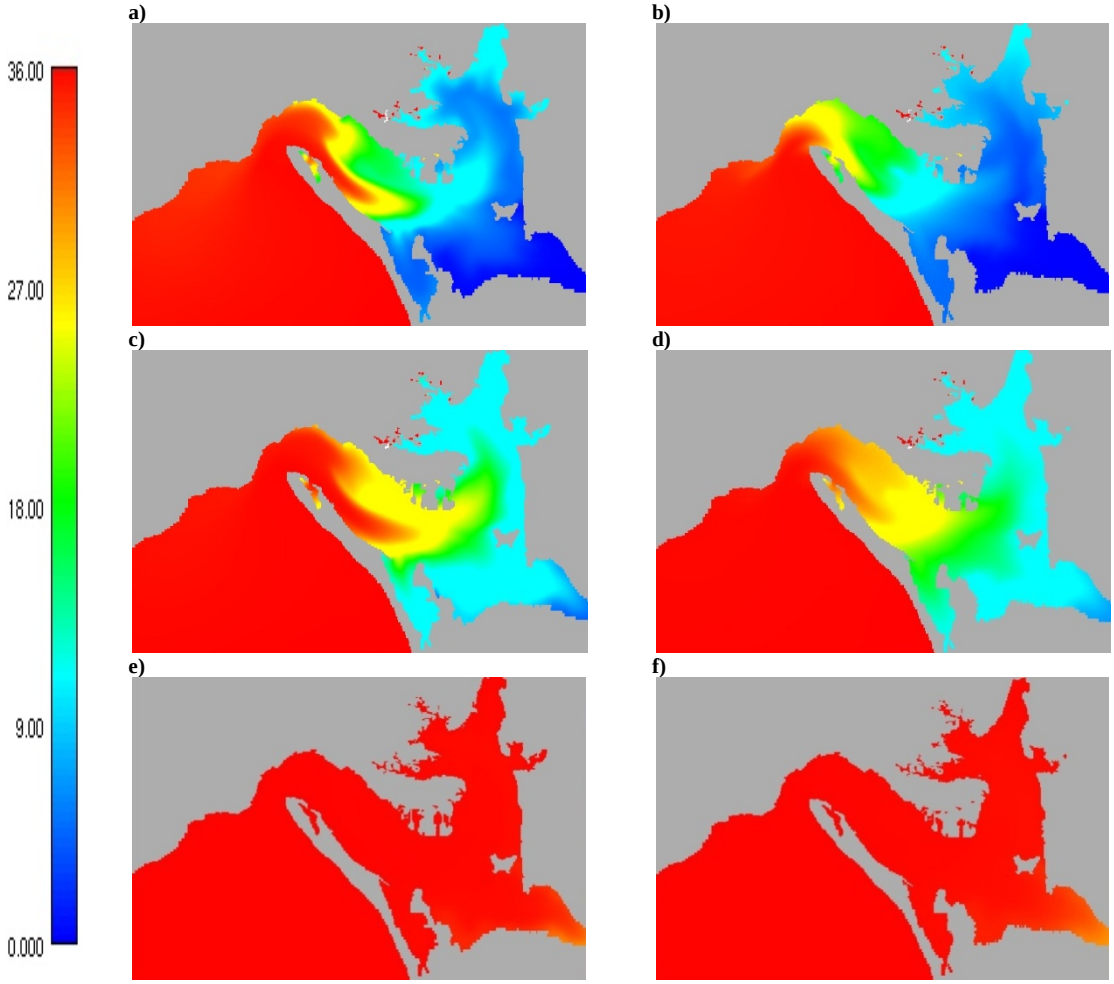

Figure 14 – Salinity fields for the Sado estuary, all figures represent high tide with bottom friction 0.0025 $m^{(1/3)}s^{-1}$: a) Q=200 m^3/s, spring tide b) Q=200 m^3/s, neap tide c) Q=50 m^3/s, spring tide d) Q=50 m^3/s, neap tide e) Q= 2 m^3/s, spring tide f) Q=200 m^3/s , neap tide.

For ebb tide it is possible to observe the progression of the mixture zone (≈9-30 psu) westerly, reaching the mouth, more evident for Q=50 m^3s^{-1} (Figures 15c) and d) than for Q= 200m^3s^{-1} (Figures 15a) and b) and reaching the ebb jet further for spring tide (Figures 15a) and c) - 30-32 psu) than for neap tide (Figures 15 b) and d) in both simulations. The river inflow effect (0-9psu) it is also enhanced for Q= 50m^3s^{-1} reaching further into the estuary than for Q= 200m^3s^{-1}. For Q=2 m^3s^{-1} there are no significant changes to analyze.

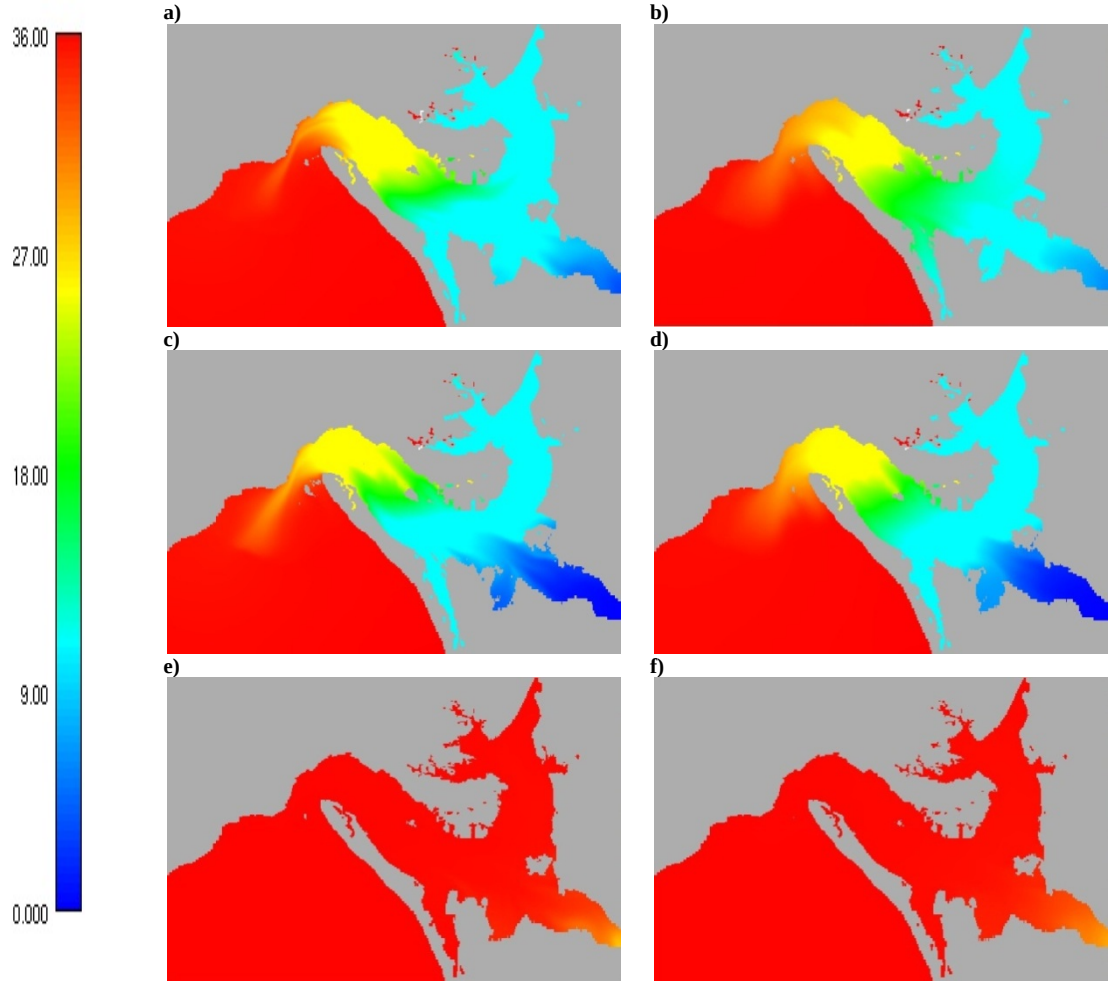

Figure 15 - Salinity fields for the Sado estuary, all figures represent the ebb with bottom friction 0.0025 $m^{(1/3)}s^{-1}$ for: a) Q=200 m^3/s, spring tide b) Q=200 m^3/s, neap tide c) Q=500 m^3/s, spring tide d) Q=50 m^3/s, neap tide e) Q=2 m^3/s, spring tide f) Q=200 m^3/s , neap tide.

Observing the salinity horizontal structure for low tide for the simulation with a river inflow of 200 m^3s^{-1} (Figures 16a) and b)) the ebb jet is clearly stronger extending further into the ocean than the one detected in Figures 15a) and b). Values are considerably smaller (≈27) showing the progression of the mixture zone westerly with the ebb tide, more evident again for spring tide (Figures 16a) and c)) than for neap tide (Figure 16b) and d)). As for Q=50 m^3s^{-1} (Figures 16c) and d)), the ebb jet is well defined as well but with higher values (≈30). The river inflow influence is considerably higher for Q=200 m^3s^{-1} once it reaches far

downstream than for Q=50 m^3s^{-1}; values of 0-9 psu can be detected for Q=200 m^3s^{-1} (Figures 15a) and b)) accompanying Tróia shoreline and almost reaching the mouth (more evident for spring tide than for neap tide) while for Q=50 m^3s^{-1} the salinities for the same area are 9-18 psu. The north arms hardly reaches values below 9 psu for Q=50 m^3s^{-1} while for Q=200 m^3s^{-1} are observed values <9 psu in the southern region of the north arm.

To notice that for a river inflow of 200 m^3s^{-1} (Figures 16a) and b)), are identified two regions in the estuary that behave very differently in terms of salinity: one which accompanies the city shoreline (North estuary) with higher salinities (>9 psu) which as coastal lagoon characteristics, and the other with low salinities (<9 psu) characteristic of a typical long and narrow estuary, which accompanies the Tróia shoreline (South estuary).

For a low value of river inflow of 2 m^3s^{-1} (Figures 16e) and f)) the salinity horizontal structure is similar to the observed for the other tidal instant analysed, only showing higher values (27-33 psu) for the entrance of freshwater into the estuary.

Still three areas can be defined, oceanic influenced, river inflow influenced and mixture, only in this case they are locate downstream the estuary and not upstream as seen for high tide (Figure 14).

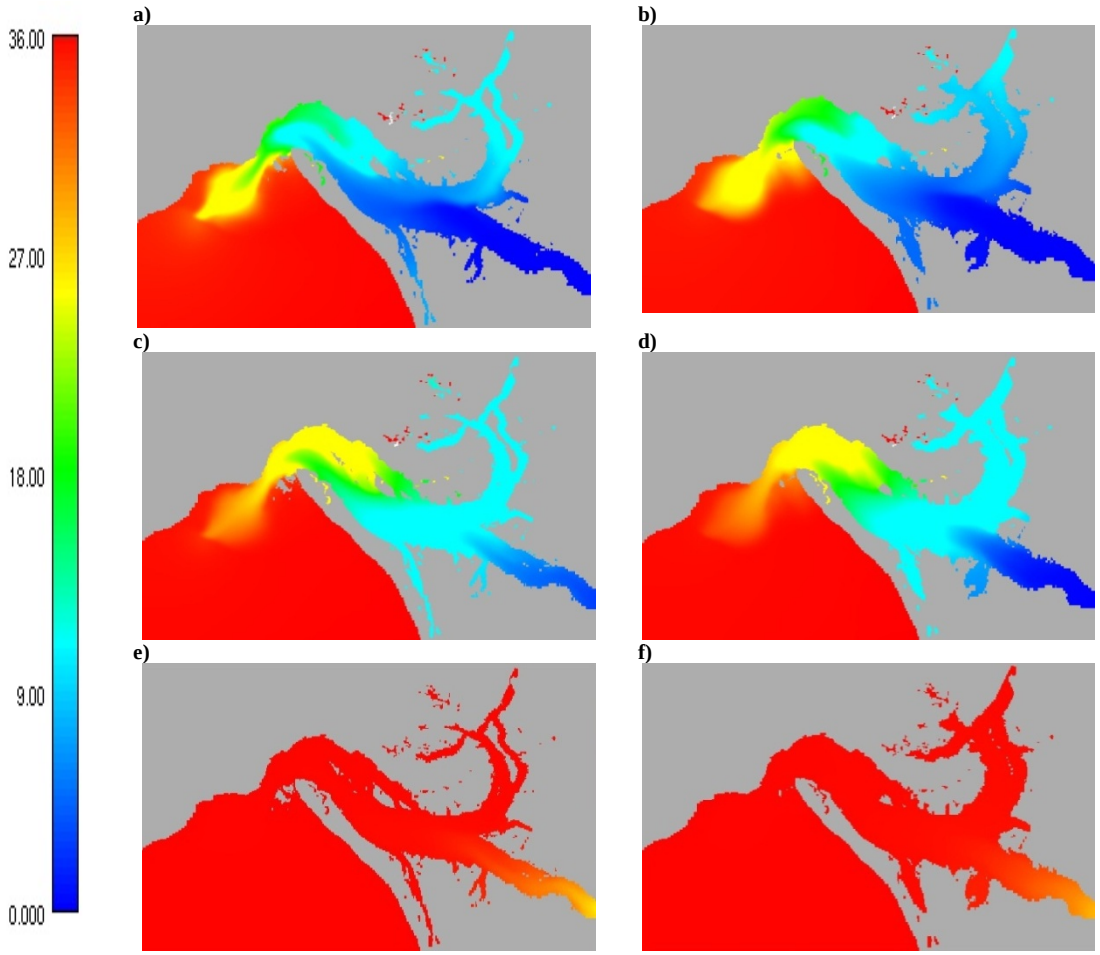

Figure 16 - Salinity fields for the Sado estuary, all figures represent the low tide and with bottom friction 0.0025 $m^{(1/3)}s^{-1}$ for:
a) Q=200 m^3/s, spring tide b) Q=200 m^3/s, neap tide c) Q=500 m^3/s, spring tide d) Q=50 m^3/s, neap tide e) Q=2 m^3/s, spring tide f) Q=200 m^3/s , neap tide.

The salinity horizontal structure for the flood is quite similar to the one presented for the ebb but with a reverse salinity gradient direction, meaning, the jet observed for ebb tide in this case is a flood jet and is entering the estuary with values of 36 psu. It reaches far into the estuary for Q=50 m^3s^{-1} than for Q=200 m^3s^{-1}. Again the values are higher for spring tide than for neap tide (in the same order than the ones observed for ebb). The river inflow entrance in the estuary it is more evident for Q=200 m^3s^{-1} than for Q=50 m^3s^{-1} and the mixture zone affects upstream the estuary for Q=50 m^3s^{-1} than for Q=200 m^3s^{-1}. For Q=2 m^3s^{-1} there are no significant changes to analyze.

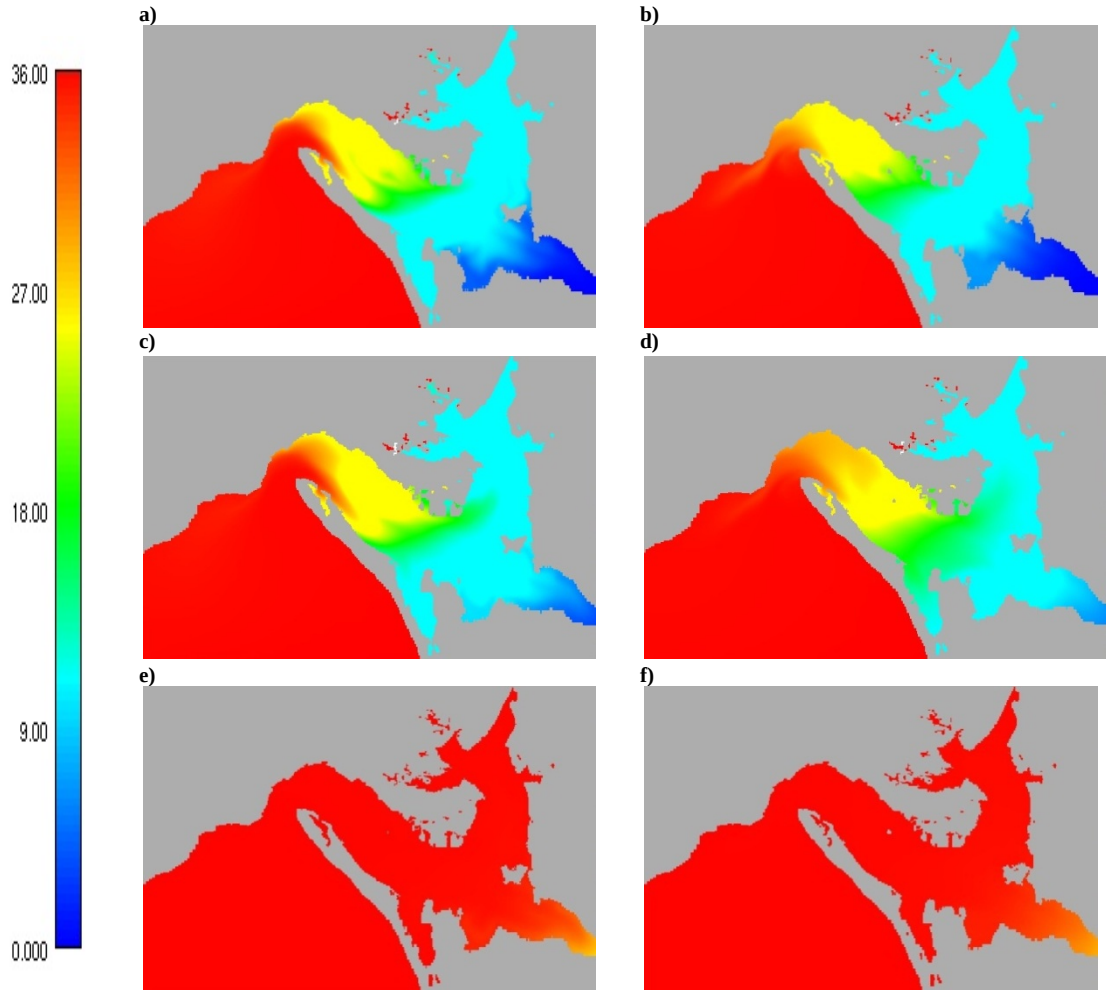

Figure 17 – Salinity fields for the Sado estuary, all figures represent the flood with bottom friction 0.0025 $m^{(1/3)}s^{-1}$: a) Q=200 m^3/s, spring tide b) Q=200 m^3/s, neap tide c) Q=500 m^3/s, spring tide d) Q=50 m^3/s, neap tide e) Q=2 m^3/s, spring tide f) Q=200 m^3/s , neap tide.

3.3. Fecal coliforms

In order to analyse the fecal coliform distribution in Sado estuary, three situations are described in terms of river inflow: 200 m^3s^{-1}, 50 m^3s^{-1} and 2 m^3s^{-1} and compared for fixed bottom friction 0.0025 $m^{(1/3)}s^{-1}$. Two discharge point where simulated (Outão and ETAR – see Figure 9 – where usually fecal coliforms discharges occur periodically) with different inflow: 0.22 m^3s^{-1} and 2.22 m^3s^{-1}. These values were chosen in order to simulate typical and extreme values of coliforms discharge, evaluating their distribution and propagation into the estuary, aiming to identify possible affected regions.

Observing figures for the discharge inflow of 0.22 m^3s^{-1}, for low and high tide (Figures 19 and 20) and ebb and flood (Figures 18 and 19) the discharges points, for all the cases, present as maximum value 1900MPN/100 ml (being 1×10^5/100 ml the initial value used for simulations).

The general horizontal fecal coliform dispersion structure for low and high tide is similar, showing a relatively small area affected by the discharges. The area affected for Outão is smaller (generally doesn't

extend more than a 1-2 km - upstream/downstream depending on the tide instant), than for ETAR, which can reach 2-4 km of plume despite the low values observed. In this case, the maximum value at the discharges point (1900MPN/100 ml) is rapidly diluted to 950-475MPN/100 ml in the surrounding area.

These values are all above maximum recommendable legislated value, but below maximum admissible legislated value (Table 2).

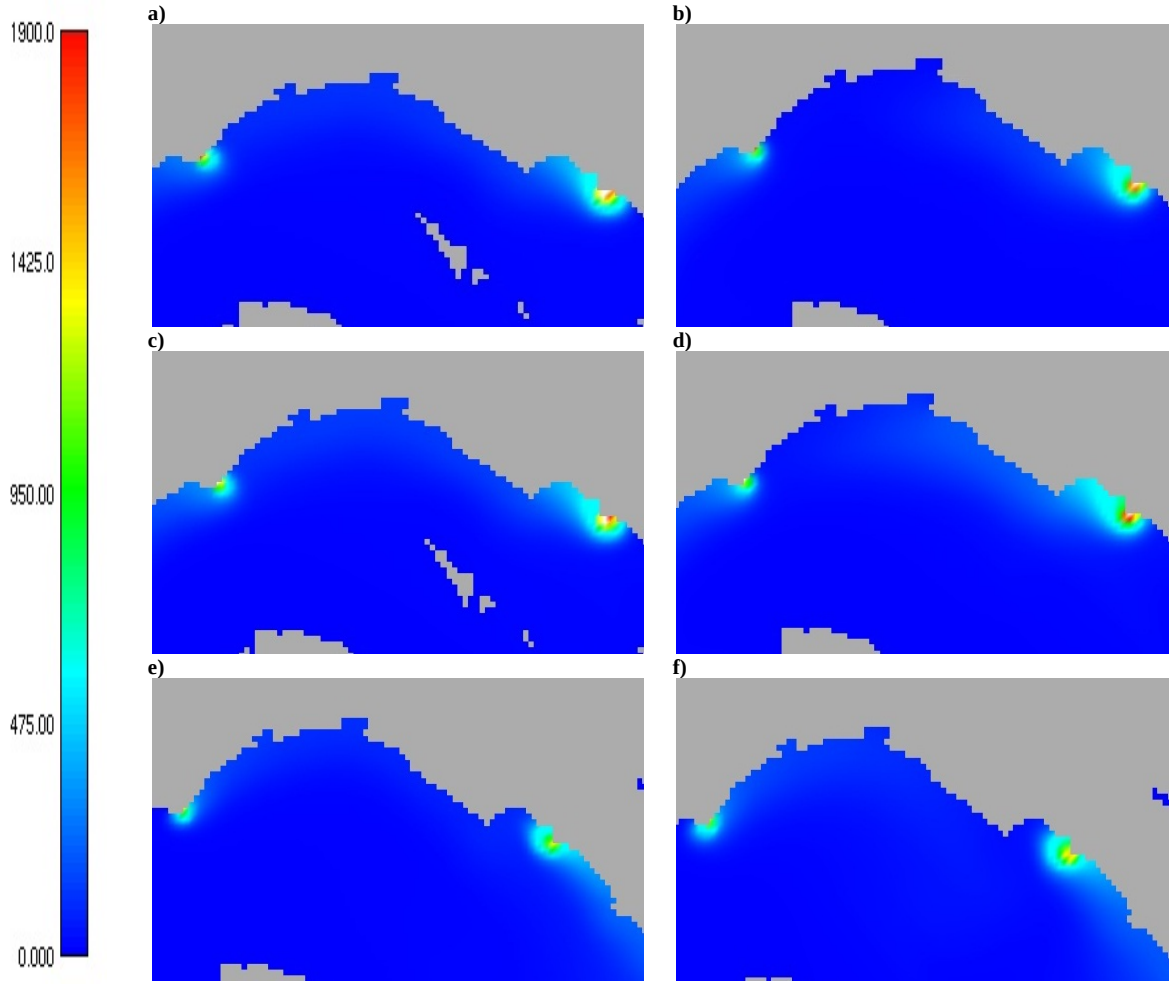

Figure 18 - Fecal coliform dispersion (MPN/100ml) for the Sado estuary with fixed discharge=0.22 m^3s^{-1}, all figures represent the low tide and with bottom friction 0.0025 $m^{(1/3)}s^{-1}$ a) Q=2 m^3s^{-1}, spring tide b) Q=2 m^3s^{-1}, neap tide c) Q=50 m^3s^{-1}, spring tide d) Q=50 m^3s^{-1}, neap tide e) Q=200 m^3s^{-1}, spring tide f) Q=200 m^3s^{-1}, neap tide. MPN – number of cells.

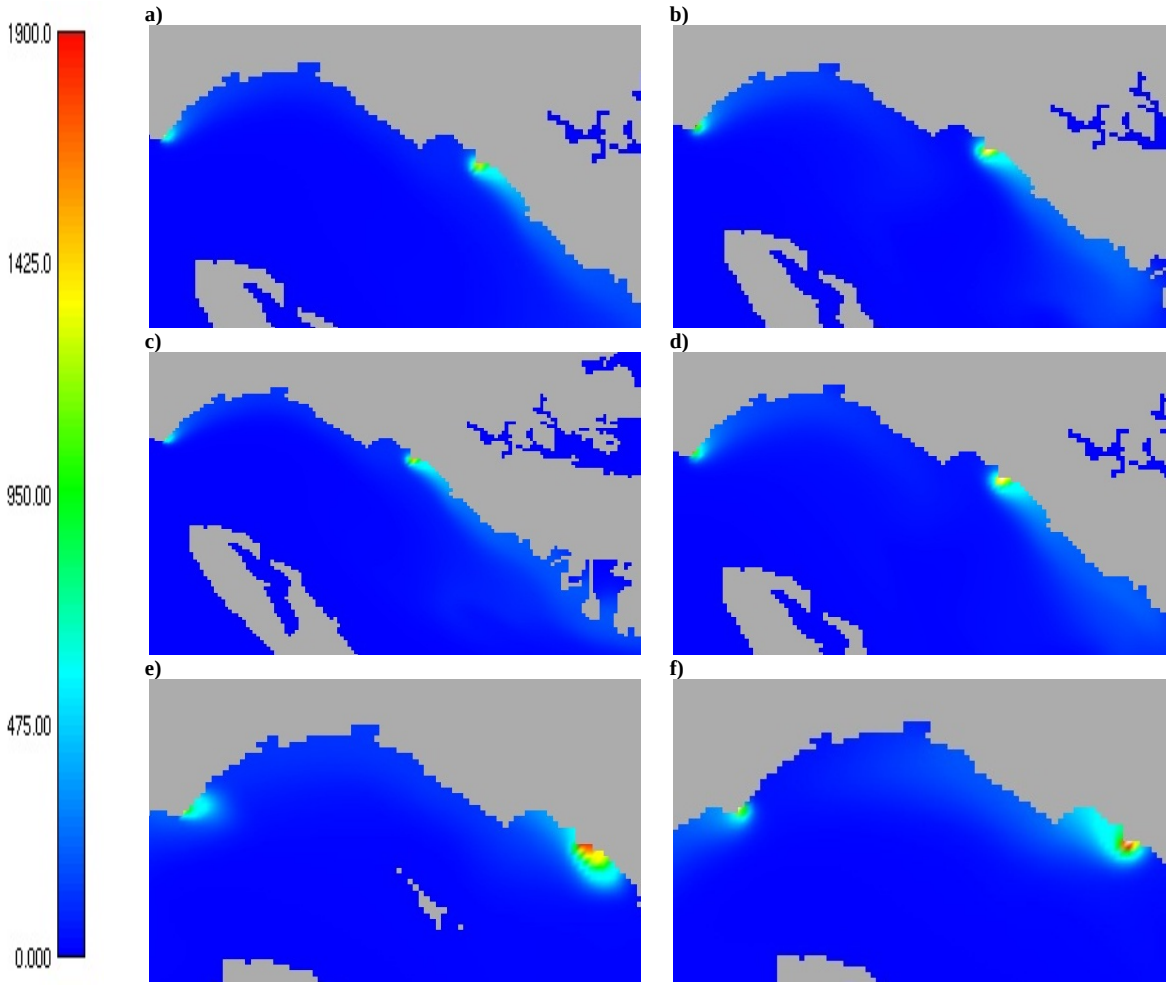

Figure 19 - Fecal coliform dispersion (MPN/100ml) for the Sado estuary with fixed discharge=0.22 m^3s^{-1}, all figures represent the high tide and with bottom friction 0.0025 $m^{(1/3)}s^{-1}$ a) Q=2 m^3s^{-1}, spring tide b) Q=2 m^3s^{-1}, neap tide c) Q=50 m^3s^{-1}, spring tide d) Q=50 m^3s^{-1}, neap tide e) Q=200 m^3s^{-1}, spring tide f) Q=200 m^3s^{-1}, neap tide. MPN – number of cells.

For ebb and flood (Figures 20 and 21), comparing with the values for the low and high tide cases they are smaller at both discharge points (Outão and ETAR), <950MPN/100 ml for ebb and <1425MPN/100 ml for flood, all being rapidly diluted as well.

The fecal coliforms concentration is slightly higher in neap tide (Figures 20 b), d) and f) and Figures 21b), d) and f)) than on spring tide (Figures 20a), b) and e) and Figure 21a), c) and e)), and this effect is more obvious for the flood.

The "*plume*", created by the dispersion induced by the tidal current, is smaller and with a higher concentration for neap tide and expands further upstream accompanying the shoreline, for flood spring tide. For ebb the behaviour is similar but the "*plume*"extends downstream towards the estuary mouth reaching higher distances than for spring tides.

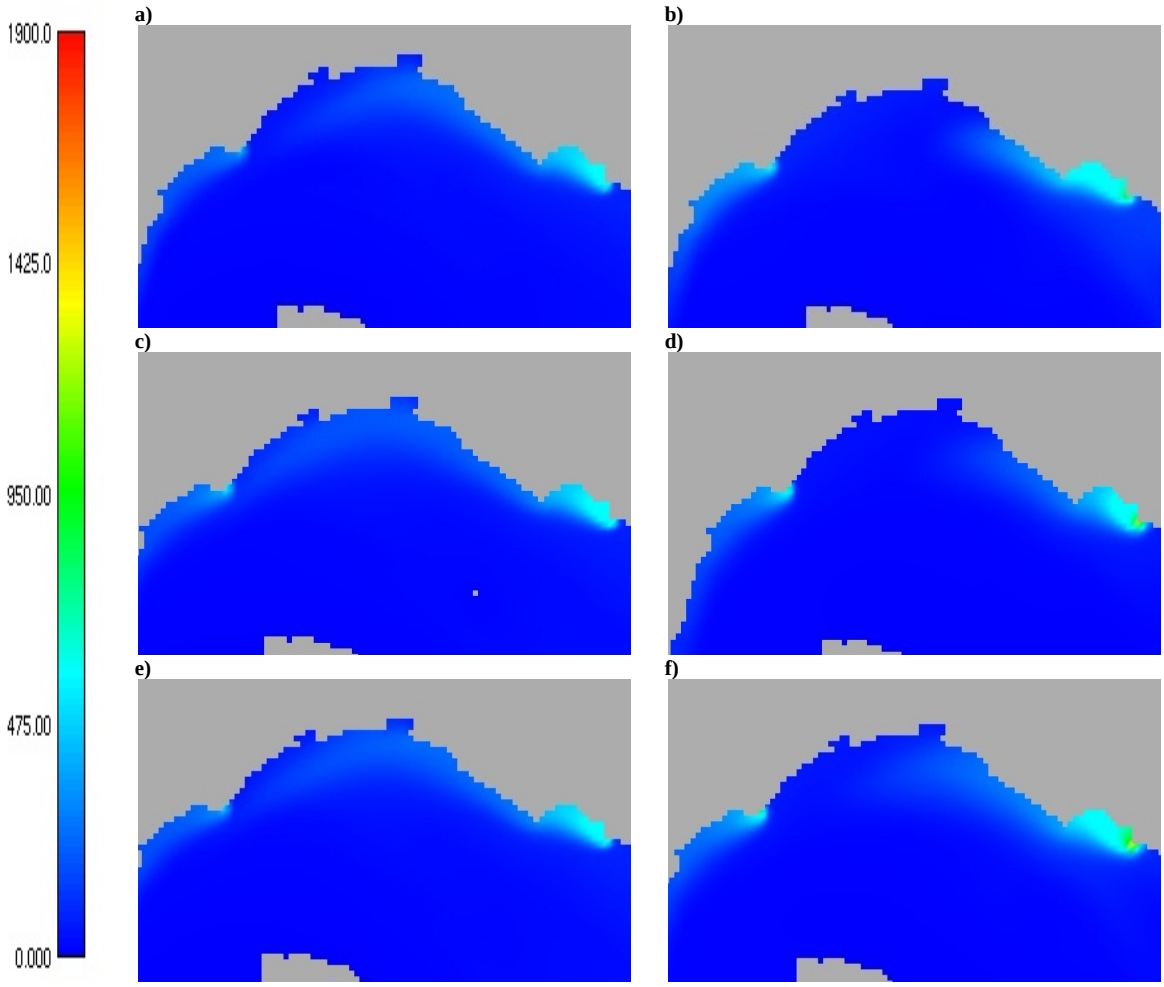

Figure 20 - Fecal coliform dispersion (MPN/100ml) for the Sado estuary with fixed discharge=0.22 m^3s^{-1}, all figures represent the ebb and with bottom friction 0.0025 $m^{(1/3)}s^{-1}$: a) Q=2 m^3s^{-1}, spring tide b) Q=2 m^3s^{-1}, neap tide c) Q=50 m^3s^{-1}, spring tide d) Q=50 m^3s^{-1}, neap tide e) Q=200 m^3s^{-1}, spring tide f) Q=200 m^3s^{-1}, neap tide. MPN – number of cells.

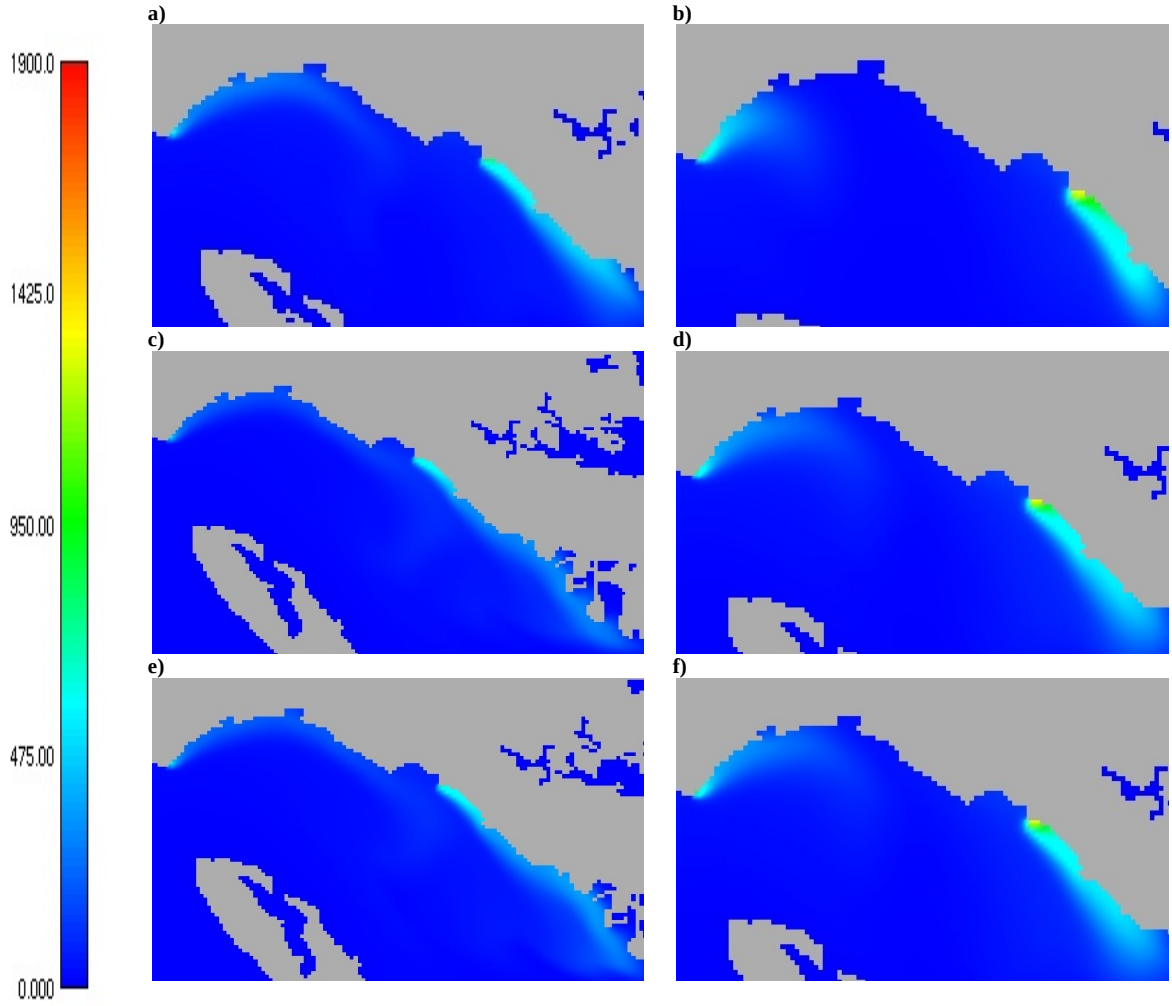

Figure 21 - Fecal coliform dispersion (MPN/100ml) for the Sado estuary with fixed discharge=0.22 m^3s^{-1}, all figures represent the flood and with bottom friction 0.0025 $m^{(1/3)}s^{-1}$: a) Q=2 m^3s^{-1}, spring tide b) Q=2 m^3s^{-1}, neap tide c) Q=50 m^3s^{-1}, spring tide d) Q=50 m^3s^{-1}, neap tide e) Q=200 m^3s^{-1}, spring tide f) Q=200 m^3s^{-1}, neap tide. MPN – number of cells.

Figures 22 and 23 (low and high tide) and Figures 24 and 25 (ebb and flood) present the horizontal structure of coliform dispersion for a sewage discharge of 2.22 m^3s^{-1}. In the discharges points are observed maximum values of 20000 MPN (being 1×10^5/100 ml the initial value used for the simulations). The horizontal distribution of fecal coliform for all situations is clearly identical, but only the focus of the discharge point present higher values than the ones observed for the lower discharge inflow (0.22 m^3s^{-1}), once the discharge values used are ten times higher.

The high sewage discharge of 2.22 m^3s^{-1}, which simulated a possible disaster scenario, showed to be quickly fade to the minimum admissible by law (<2000) in a small area near the discharge point.

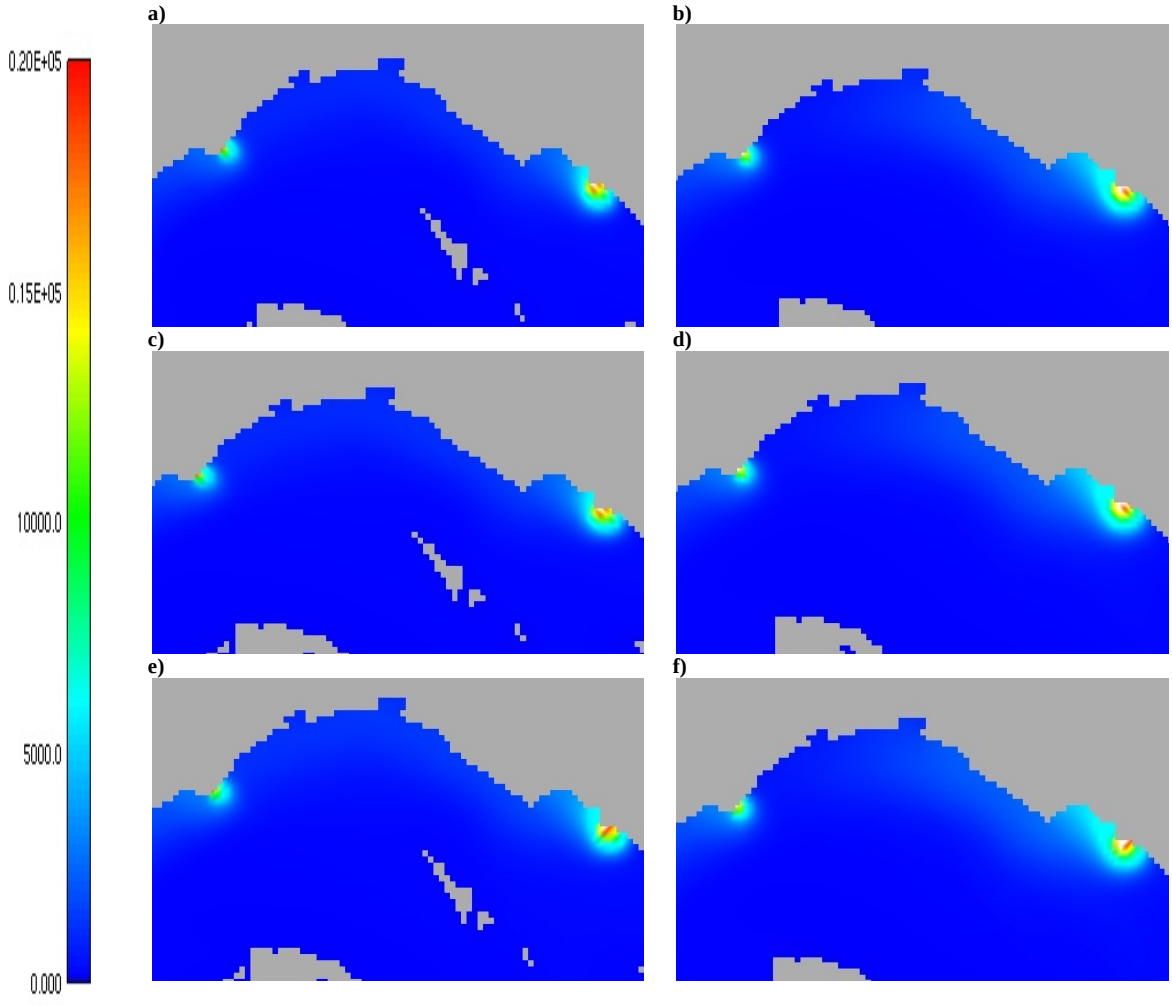

Figure 22 – Fecal coliform dispersion (MPN/100ml) for the Sado estuary with fixed discharge=2.22 m^3s^{-1}, all figures represent low tide and with bottom friction 0.0025 $m^{(1/3)}s^{-1}$ a) Q=2 m^3s^{-1}, spring tide b) Q=2 m^3s^{-1}, neap tide c) Q=50 m^3s^{-1}, spring tide d) Q=50 m^3s^{-1}, neap tide e) Q=200 m^3s^{-1}, spring tide f) Q=200 m^3s^{-1}, neap tide. MPN – number of cells.

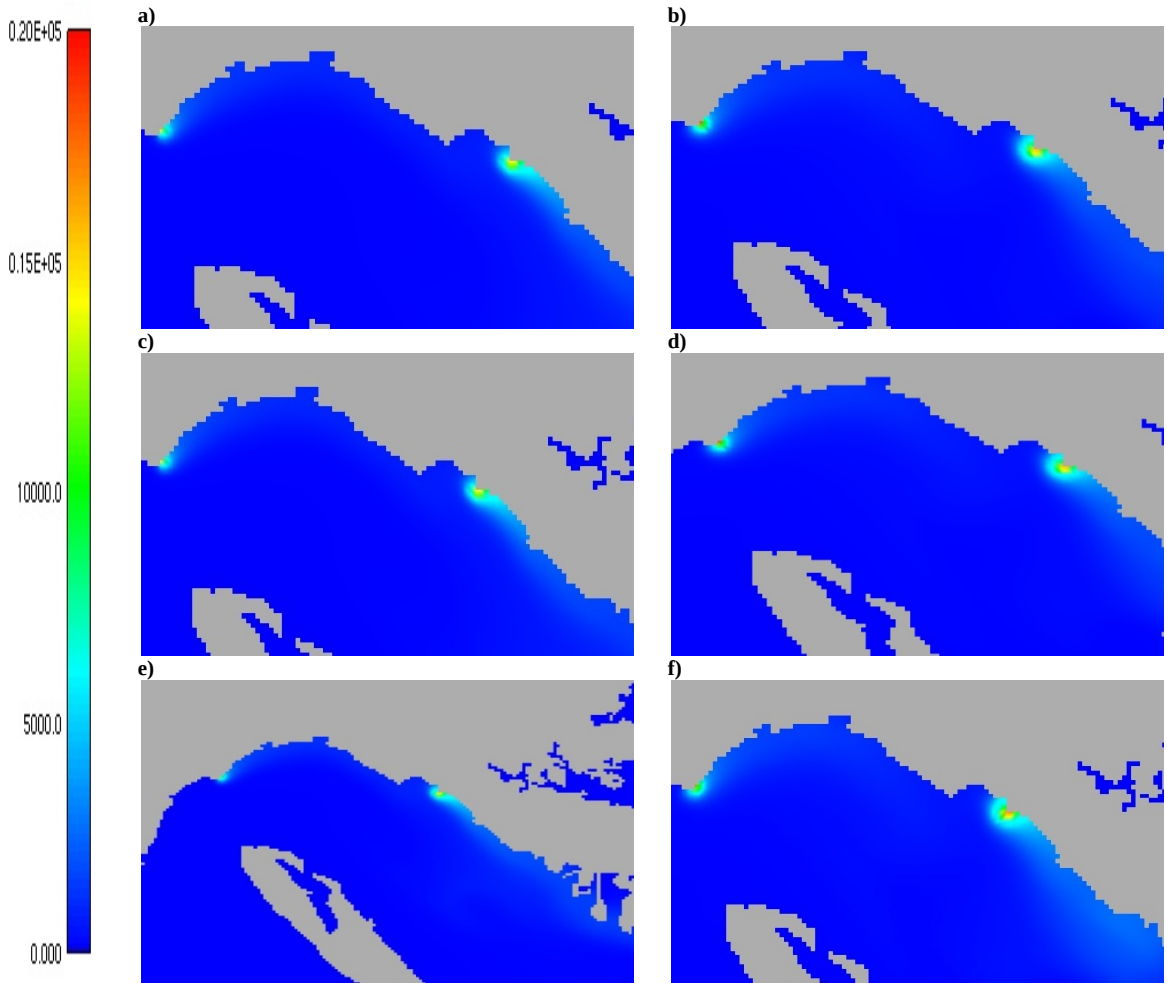

Figure 23 - Fecal coliform dispersion (MPN/100ml) for the Sado estuary with fixed discharge=2.22 m^3s^{-1}, all figures represent high tide and with bottom friction 0.0025 $m^{(1/3)}s^{-1}$ a) Q=2 m^3s^{-1}, spring tide b) Q=2 m^3s^{-1}, neap tide c) Q=50 m^3s^{-1}, spring tide d) Q=50 m^3s^{-1}, neap tide e) Q=200 m^3s^{-1}, spring tide f) Q=200 m^3s^{-1}, neap tide. MPN – number of cells.

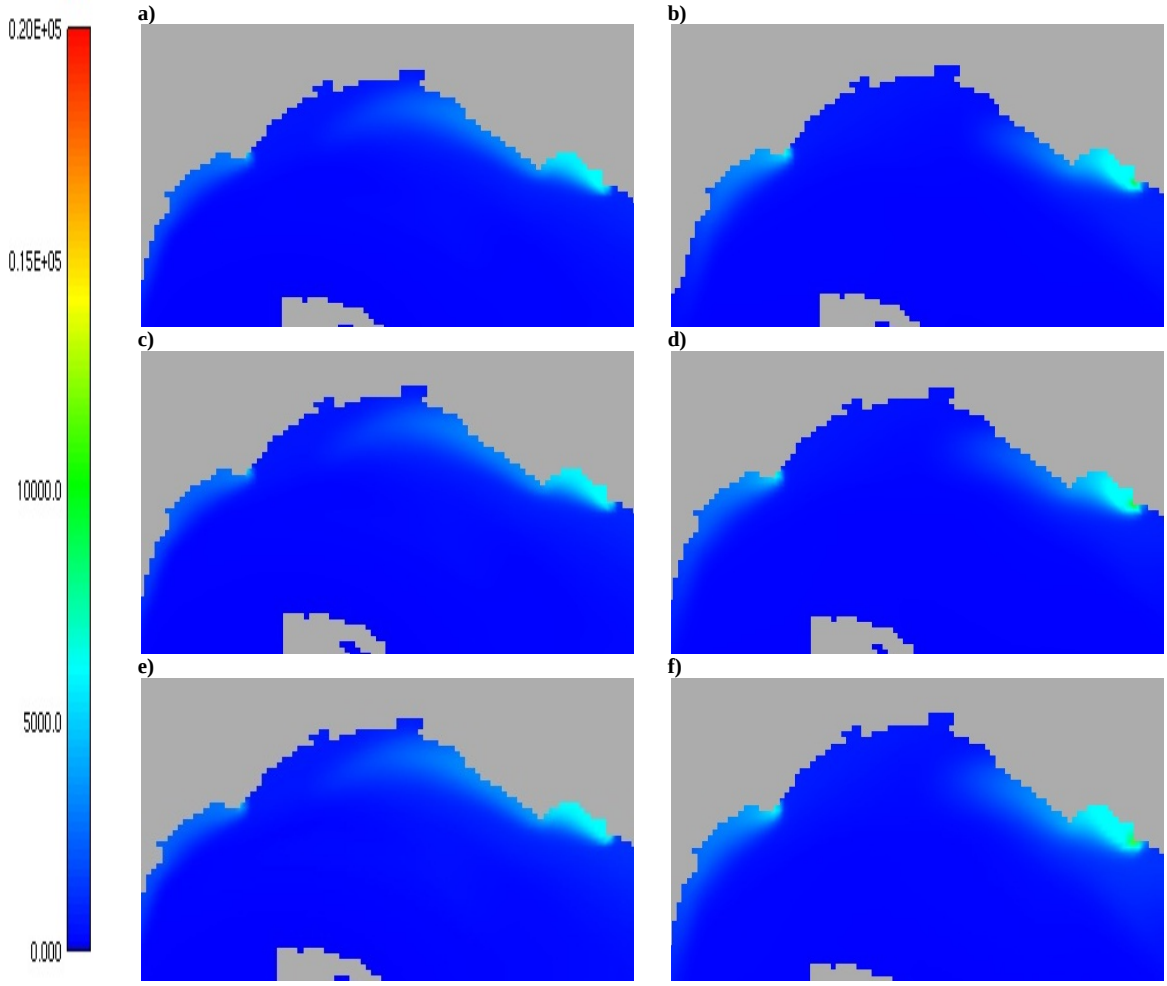

Figure 24 - Fecal coliform dispersion (MPN/100ml) for the Sado estuary with fixed discharge=2.22 m^3s^{-1}, all figures represent ebb and with bottom friction 0.0025 $m^{(1/3)}s^{-1}$ a) Q=2 m^3s^{-1}, spring tide b) Q=2 m^3s^{-1}, neap tide c) Q=50 m^3s^{-1}, spring tide d) Q=50 m^3s^{-1}, neap tide e) Q=200 m^3s^{-1}, spring tide f) Q=200 m^3s^{-1}, neap tide. MPN – number of cells.

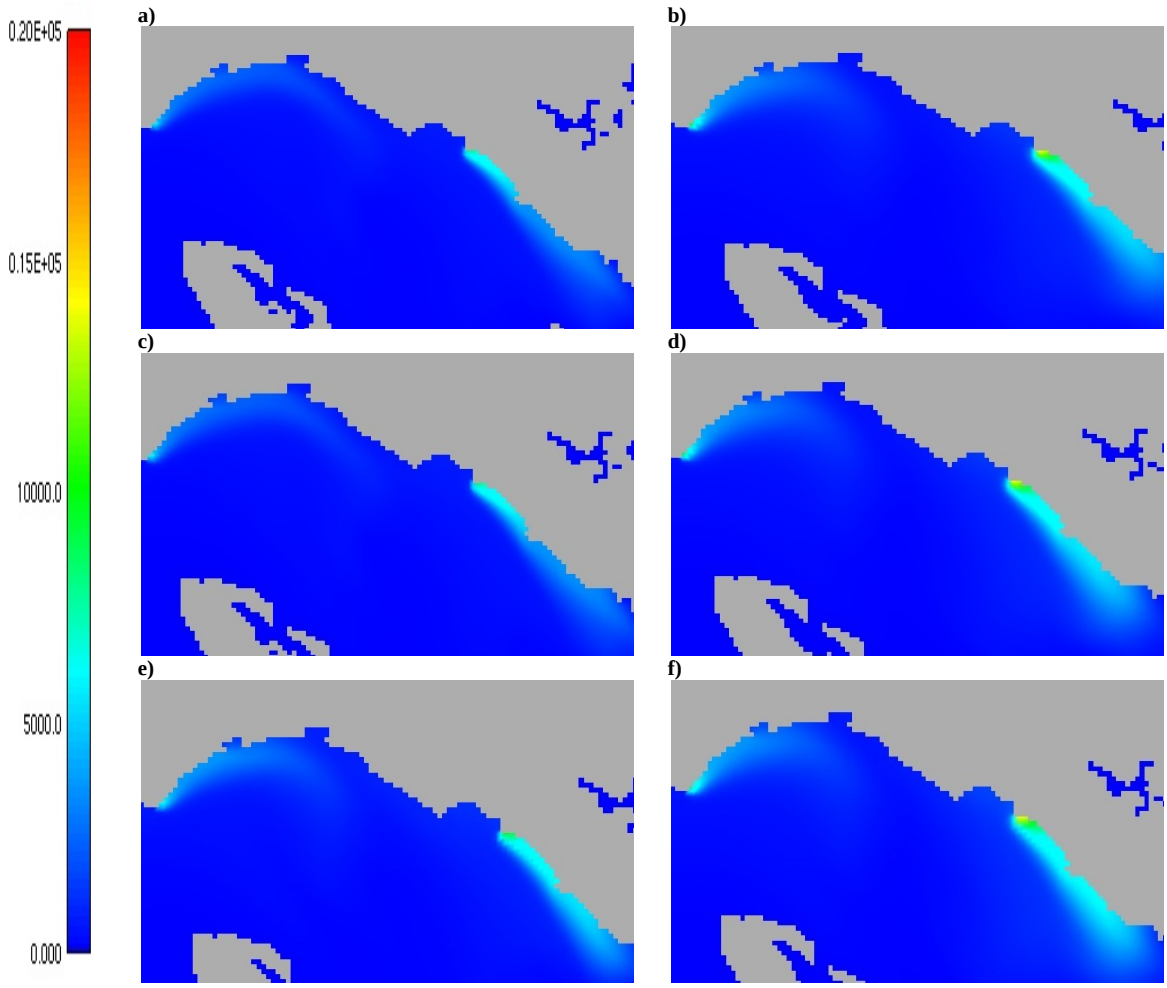

Figure 25 - Fecal coliform dispersion (MPN/100ml) for the Sado estuary with fixed discharge=2.22 m^3s^{-1}, all figures represent flood and with bottom friction 0.0025 $m^{(1/3)}s^{-1}$ a) Q=2 m^3s^{-1}, spring tide b) Q=2 m^3s^{-1}, neap tide c) Q=50 m^3s^{-1}, spring tide d) Q=50 m^3s^{-1}, neap tide e) Q=200 m^3s^{-1}, spring tide f) Q=200 m^3s^{-1}, neap tide. MPN – number of cells.

Acording to the Sado Hidrographic Bay Plan [Plano da Bacia Hidrográfica do Rio Sado, 2001], the residual waters with origin in Setúbal are an important source of the microbiological estuarine communities. The reduced dilution capacity of these areas, quoted by the same plan, leaded to high pollutant concentrations. In terms of industry, the principal potential pollutants, according to the same study, are SETENAVE (shipyard), PORTUCEL/INAPA (producers of stock paper and derivates), SAPEC (fertilizers, pesticides and chemical products) and the Thermal Central of Setúbal which had the major discharges (equal to the ETAR used in this work). The major pollutant activities (industries and port activities) were located in the North estuary channel and the estimated total punctual load of industrial origin discharged directly in the waterlines was estimated as: Total Coliforms=5.24×10^{15}PMN and Fecal Coliforms=5.24×10^{15}PMN, values considerably higher than the obtained results obtained in this work.

According to conclusions of a study performed by Rodrigues & Quintino [1987], the industrial pollution, with no treatment at all, that affected Sado estuary (North channel) was enormous, affecting ≈660 thousand citizens. The data revealed that in this estuarine area (North channel), the waters showed low transparency,

less oxygen and higher temperatures than in the South estuary arms. Comparing to the Outão area, the waters presented higher quality than the ones in the North channel, although the medium values obtained for the various parameters controlled in the study for superficial and bottom waters fulfilled the legislated values (Decreto-Lei 74/90).

The same study concluded that river waters had no influence in the estuary water quality, despite the punctual pollution detected across the study area. In the contrary, the estuary gave a positive influence over the river water quality, which implied a decrease of the nutrients and suspended solids concentration representing a high transparency in the flooding and higher oxygenation downstream Alcácer. It is reasonable to conclude that this was due to dilution effect caused by the entrance of large oxygenated water masses with low nutrient concentrations.

Regarding the microbiological water quality, the INETI laboratory developed a study from July 1986 to December 1988, which includes the North and South estuary channels. The results of this study pointed to high levels of microbiological pollution in the North arm, in the areas close to the discharge industrial effluents, namely PROPAM, and discharges from residual waters of urban origin (Setúbal). In the South arm, at the mouth and upstream the estuary, the pollution levels were considerably lower. The obtained results revealed the tendency of the bacterial concentration to decrease upstream and downstream the estuary. All these statements justify the choice of OUTÃO and ETAR as the discharge sewage points to simulate in this work.

Although some data are available, they are not enough [Relatório de Actividades, 2005] to elaborate the “big picture” of the water quality in the Sado estuary bay. The largest part of the available data is shaped for the water quality analysis for human consume. However, it is possible to recognize a huge temporal and spatial variability associated to the seasonal river runoff, to high physiographic bay irregularities and to irregular pollution sources distribution. The available information is not enough to evaluate the overall evolution quality, but is reasonable to consider that is in agreement with the pollution sources distribution.

Although the results seem to describe some of the patterns previously found, the available data are too old to be considered representative the actual estuarine behavior, once many modifications occurred after the completion of those studies (see Annex 4 – contains several studies and the year they were conducted). In terms of sewage treatment, industries, residual city sewage, number of citizens, etc. the reports described above already had concluded that there is a huge lack of data to perform this kind of studies.

IV. CONCLUSIONS - FINAL CONSIDERATIONS

The major objectives of this work were to study the hydrodynamics/hydrography and distribution/dispersion of fecal coliforms in the Sado estuary, using the numerical model MOHID, which was implemented in a 2D mode due to the estuary characteristics (low depth and strong tidal currents).

- ✓ When the river inflow is weak (2 m^3/s), the hydrodynamics/hydrography of the estuary is clearly tidal dominated, but when the river inflow is high (200 m^3/s), the horizontal patterns of salinity inside the estuary are determined by a balance between tide and river inflow effects. In this case it is found a classic division of the estuary in three distinct regions: marine, mixing and freshwater. It was found that the tide inside the estuary is semi-diurnal, presenting M_2 and S_2 as the principal tidal constituents.

- ✓ The estuary topography influence (related to bottom friction) revealed, as expected, an important role in the estuary dynamics, once the horizontal velocity structure as well as the spectral and harmonic analysis results showed different behaviors with higher and lower Manning values.

- ✓ Despite the significant estuarine dynamics, the concentration of fecal coliforms was found confined to small areas close to the discharge points. These organisms were found to affect only restricted areas near the sewage stations for a discharge flow of 0.22 m^3/s, with concentrations fulfilling the legislated values, found just after the discharge points and along the estuary. With a discharge flow typical of a disaster scenario (2.22 m^3/s), the pattern found was similar. The discharge flow was 10 times larger, but the fecal coliform concentration was rapidly diluted, once the river had the capacity to absorb quickly these huge concentrations.

- ✓ Despite all the conclusions taken above, it is important to understand that there is a huge lack of the data required to perform this kind of studies. The available data have approximately 20 years or more (see Annex 4, Table 15 that shows a compilation of the last studies conducted in Sado estuary), and the estuary hydrodynamics/hydrographic conditions hardly will be those nowadays. Although there are some recent events, namely the return of female dolphin with infant and otters that lately have been seen again in the estuary channels showing that still subsist areas with good water quality.

Future work:

In the future, it becomes extremely important to perform several experimental studies in order to increase and renew the knowledge about Sado estuary dynamics (chemical, physical and other variables). It will be useful to perform field surveys that cover spring-neap cycles in order to evaluate the fortnight variation of the salinity, water temperature and current velocity and to carry out a spatial/temporal coverage of endangered areas like the Northern channel, where most critical industries can be found. Furthermore, studies of bacterial presence in the estuary and main channels are suggested.

All these studies will be useful to evaluate new implementations of numerical models, which will aim to fulfill the gaps of *in situ* available data. Is expected that these new numerical models will produce more accurate results, helping to the correct understanding of the estuarine biogeochemical processes in order to resolve and prevent ecological problems associated with the human activity.

V. REFERENCES

Alvarez I., deCastro M., Gomez-Gesteira M., Prego R., 2005; Inter- and intra-annual analysis of the salinity and temperature evolution in the Galician Rias Baixas-ocean boundary (northwest Spain), *Journal of Geophysical Research* **110**, doi: 10.1029/2004JC002504,

Alvarez I., deCastro M., Prego R., Gómez-Gesteira M., 2003; Hydrographic characterization of a winter-upwelling event in the ria of pontevedra (NW Spain), *Estuarine Coastal and Shelf Science* **56**, 869–876.

Ambar I., Fiuza A., Sousa M., Lourenço I., 1980; General circulation in the lower Sado river estuary under drought conditions, *Seminario sobre problemas actuais de oceanografia em Portugal*, INVOTAN, lisboa, 4p.

Backhaus J., 1983; A semi-implicit scheme for the shallow water equations for application to shelf sea modeling, *Continental Shelf Sea Research* **2**, pp. 243–254.

Braunschweig F., Martins F., Chambel P., Neves R., 2003; A methodology to estimate renewal time scales in estuaries: the tagus estuary case, **Ocean Dynamics 53**, pp. 137–145.

Braunschweig F., Chambel P., Fernandes L., Pina P., Neves R., 2004; The object oriented design of the integrated modelling system MOHID, *Proceedings of the XVth International Conference on Computational Methods in Water Resources (CMWR XV)*, June 13–17, Chapel Hill, NC, USA.

Braunschweig F., Fernandes L., Galvão P., Trancoso R., Pina P., Neves R., 2005; MOHID GIS—A geographical information system for water modeling software, *Geophysical Research Abstracts*, EGU Meeting 05-A-08213, 25–29 April, Wien, Austria.

Brock T. D., 1981. Calculating solar radiation for ecological studies. Ecological Modelling.

Burchard H., Bolding K., Villarreal M. R., 1999; GOTM, a general ocean turbulence model, *scientific documentation technical report*, European Community, Ispra, Italy.

Cabeçadas L., 1993; Ecologia do fitoplâncton do estuário do Sado: para uma estratégia de conservação, *Estudos de Biologia e Conservação da Natureza* **10**, Instituto de Conservação da Natureza, Lisboa.

Caeiro S., Painho M., Goovaerts P., Costa H., Sousa S., 2003; Spatial sampling design for sediment quality assessment in estuaries, *Science Direct-ELSEVIER, Environmental Modelling & Software* **18**, pp. 853–859.

Cameron W.M., Pritchard D.W., 1963; Estuaries. In: Hill, *M.N. (Ed.), The Sea*, **vol. 2**. Wiley, New York, pp. 306 and 324.

Cancino L., Neves R., 1999; Hydrodynamic and sediment suspension modelling in estuarine systems. Part II: Application to theWestern Scheldt and Gironde estuaries, *Journal of Marine Systems* **22**, pp. 117–131.

Chapra S. C., 1997; Surface Water Quality Modeling, *Civil engineering series*, McGraw-Hill.

deCastro M., Gomez-Gesteira M., Alvarez I., Prego R., 2004; Negative estuarine circulation in the Ria of Pontevedra (NW Spain), *Estuarine Coastal and Shelf Science* **60**, pp. 301–312.

Defant A., 1960; Physical oceanography, Oxford, Pergamon Press. **v. 2.**

Dias J., Sousa M., Bertin X., Fortunato A., Oliveira A., 2009; Numerical modeling of the impact of the Ancão Inlet relocation - Ria Formosa, Portugal, *Environmental Modelling & Software* **24**, pp. 711–725,.

Doyle M., Erickson M., April 2006; The fecal coliform assay, the results of which have led to numerous misinterpretations over the years, may have outlived its usefulness, *Microbe*, **vol.1,** nº 4.

Dronkers J. J., 1964; Tidal Computations in Rivers and Coastal Waters, North-Holland Publishing Company.

Duarte A., 2006; Influência da hidrodinâmica em estuaries sujeitos a eutrofização, *Hidronet*.

Dyer K.R., 1997; *Estuaries: a physical introduction*, Second Edition. J. Wiley and Sons Ltd., Chichester, pp. 195.

Gallo M., 2004; *A Influência da vazão fluvial sobre a propagação da maré no estuário do rio Amazonas*, tese de mestrado em engenharia oceânica, pp. 1-99.

Gibson J. R., Najjar R. G., 2000; The response of Chesapeake Bay salinity to climate-induced changes in streamflow, *Limnology and Oceanography* **45**, pp. 1764–1772.

INAG/MARETEC/IST, 2002; Water Quality in Portuguese Estuaries: Mondego, Tejo and Sado.

Jenkins A. (1984) The effect of fluvial processes on the dynamics of sanitary bacteria in upland streams. Ph.D. thesis, Univ. of Leeds.

Jerlov N. G., 1968; Optical Oceanography, *Elsevier*, pp. 194.

Kjerfve B., 1989; Estuarine geomorphology and physical oceanography, *Physics of Shallow Estuaries and Bays*, J. van de Kreeke, Spring Verlag, pp. 22–29.

Kjerfve B., 1990; Manual for investigation of hydrological processes in mangrove ecosystems, *Technical report*, UNESCO/UNDP, New Dehli, pp. 79.

Kranenburg C., 1986; A timescale for long-term salt intrusion in well-mixed estuaries, *Journal of Physical Oceanography* **16**, pp. 1329–1331.

Kraus E. B., 1972; Atmosphere-Ocean Interaction, *Clarendon Press*, Oxford.

Leitão P. C., 1996; *Modelo de dispersão lagrangeano tridimensional*, Tese de Mestrado em Ecologia, Gestão e Modelação de Recursos Marinhos, Instituto Superior Técnico, Lisboa.

Leitão P. C., 2003; *Integração de Escalas e de Processos na Modelação do Ambiente Marinho*, Tese de Doutoramento, Instituto Superior Técnico. Universidade Técnica de Lisboa, Lisboa.

Leendertse J., Liu S., 1978; A three-dimensional turbulent energy model for non-homogeneous estuaries and coastal sea systems, In: Nihoul, J. (Ed.), *Hydrodynamics of estuaries and Fjords, Elsevier*, Amsterdam, pp. 387–405.

MacCready P., 1999; Estuarine adjustment to changes in river flow and tidal mixing, *Journal of Physical Oceanography* **29**, pp. 708 – 726.

Maldonado Soto Y., 2004; *A Modelagem Hidrodinâmica como apoio a tomada de decisão em caso de derrame de óleo na parte interna do complexo estuarino Antonina-Paraguá –PR*, Tese de mestrado, Universidade Federal do Paraná, Curitiba.

Martins F., Leitão P., Silva A., Neves R., 1998; 3D modelling in the Sado estuary using a new generic vertical discretization approach, Ed. V. Babovic & L. C. Larsen, Balkema, Rotterdam, *Proceedings de Hydroinformatics'98*, **Vol. 2**, pp. 1403-1410,

Martins F., 2000; *Modelação matemática tridimensional de escoamentos costeiros e estuarinos uzando uma abordagem de coordenada vertical genérica*, Tese de Doutoramento, I.S.T.

Martins F., Neves R., Leitão P., Silva A., 2001; 3D modeling in the Sado Estuary using a new generic coordinate approach, *Oceanologica Acta* **24**: S51–S62.

Martins F., Neves R., Leitão P., 2002; Simulating vertical water mixing in homogeneous estuaries: the SADO Estuary case, *Hydrobiologia* **475/476**: pp. 221 – 227.

Martins F., Neves R., Pina P., 2002; Modelação do Impacte Produzido pelo aumento de nutrientes na produção primária do estuário do Sado.

Meller A., 2004; *Simulação Hidrodinâmica integrada do Sistema de Drenagem em Santa Maria-RS*, dissertação de mestrado, Santa Maria, RS, Brasil.

Miranda L., Castro B., Kjerfve B., 2002; *Princípios de Oceanografia de Estuários*, Editora da Universidade de S. Paulo, S. Paulo, iSBN: 85-314-0675-7.

Monismith S. G., Kimmerer W., Burau J. R., Stacey M. T., 2002; Structure and flow-induced variability of the subtidal salinity field in northern San Francisco Bay, *Journal of Physical Oceanography* **32**, pp. 3003–3019.

Montero P., 1999; *Estudio de la hidrodinâmica de la ría de vigo mediante un modelo de volumenes finitos*, Ph.D. thesis, Universidad de Santiago de Compostela, Spain.

Moreira M.J., 1987; Estudo fitogeográfico do ecossistema de sapal do estuário do Sado, *Finisterra*, **XXII, 44**, Lisboa, pp.247-296.

Mourão I., Caeiro S., Costa M., Ramos T., Painho M., 2004; Application of the DPSIR model to the Sado Estuary in a GIS context – Social and Economical Pressures, Toppen F., Prastacos P. (Ed.) *Proceedings of 7th Conference on Geographic Information Science*, Crete University Press. AGILE, Crete, Greece, pp. 391 – 402.

Neill M., 2004; Microbiological Indices for total coliform and E. coli bacteria in estuarine waters, *Science Direct, Marine Pollution Bulletin* **49**, pp. 752–760.

Neves R. J., 1985; A Bidimensional Model for Residual Circulation in Coastal Zones. Application to the Sado Estuary, *Annalles Geophysicae*, **3 e 4**, pp. 465-472.

Neves R. J., 1985; *Étude Experimentale et Modélisation des Circulations Transitoire et Résiduelle dans l'estuaire du Sado*, Ph.D. thesis, University of Liège, Liège, Belgium, pp. 271.

Neves R., Martins F., 2004; *Modelação Hidrodinâmica e Ecológica no Estuário do Sado*, Universidade Nova de Lisboa (UNL).

Neves R., Chozas S., Costa L.T., Rufino R., 2004; *Reserva Natural do Estuário do Sado, uma contribuição para o plano de gestão*, Instituto da Conservação da Natureza / Centro de Zonas Húmidas.

Officer C. B., Kester D. R., 1991; On estimating the non-advective tidal exchanges and advective gravitational circulation exchanges in an estuary, *Estuarine Coastal and Shelf Science* **32**, pp. 99–103.

Oliveira A., Fortunato A. B., Pinto L., 2006; Modelling the hydrodynamics and the fate of passive and active organisms in the Guadiana estuary; *Science Direct: Estuarine, Coastal and Shelf Science* **70**, pp. 76-84.

OSPAR, 2002; *Comprehensive Procedure, PORTUGAL, Mondego, Tagus and Sado Estuaries*, MARETEC and IST, In: OSPAR Convention for the Protection of the Marine Environment of the North-East Atlantic. (Ed.). OSPAR Commission, London.

Palma E. D., Matano R. P., 1998; On the implementation of passive open boundary conditions for a general circulation model: The barotropic case, *Journal of Geophysical Research* **103**, pp. 1319–1342.

Palma E. D., Matano R. P., 2000; On the implementation of passive open boundary conditions for a general circulation model: The three-dimensional case, *Journal of Geophysical Research* **105**, pp. 8605–8627.

Paulson C. A., Simpson J. J., 1977; Irradiance measurements in the upper ocean, *Journal of Physical Oceanography* **7**, pp. 952–956.

Pawlowicz R., Beardsley B., Lentz S., 2002; Classical Tidal Harmonic Analysis including Error Estimates in MATLAB using T_TIDE, *Computers &Geosciences*, **v.28**, pp.929-937.

Pinho J., 2000; *Aplicação de Modelação Matemática ao estudo da Hidrodinâmica e da Qualidade da água em Zonas Cosateiras*, Tese de Doutoramento, Universidade do Minho.

Plano da Bacia Hidrográfica do Rio Sado, 12 de Novembro de 2001; Relatório Final.

Prego R., Dale A. W., deCastro M., Gómez-Gesteira M., Taboada J. J., Montero P., Villareal M. R., Pérez-Villar V., 2001; Hydrography of the Pontevedra Ria: Intra-annual and temporal variability in a Galician coastal system (NW Spain); *Journal of Geophysical Research* **106 (C9)**, pp. 19845–19857.

Pugh D. T., 1987; *Tides, Surges and Mean Sea Level*, John Wiley and Sons, Swindon, UK, Chichester, pp. 472.

Randall F., 2000; T*otal Maximum Daily Load (TMDL) for Fecal Coliform Bacteria in the Waters of Duck Creek in Mendenhall Valley, Alaska*.

Rebordão I., 2008; *Análise do potencial energético dos fluxos de maré no estuário do rio Lima*, dissertação de mestrado, Universidade Técnica de Lisboa, Instituto Superior Técnico.

Relatório de Actividades, 2005; Ambiente e ordenamento do território.

Ribeiro M. M., Neves R.J., 1982; *Caracterização Hidrográfica do Estuário do Sado estuário do Sado*, Technical Report Departamento de Engenharia Mecânica, I.S.T., Universidade Técnica de Lisboa, Lisboa.

Rodrigues A. & Quintino V., 1987; Estuário do Sado: estudo do efeito dos efluentes urbano-industriais sobre a macrofauna bentónica subtidal. 1 - Sedimentologia. Relatório interno do Laboratório Nacional de Engenharia e Tecnologia Industrial.

Santos A. J., 1995; *Modelo hidrodinâmico tridimensional de circulação oceânica e estuarina*, Tese de Doutoramento, Universidade Técnica de Lisboa, Lisboa, pp. 273.

Servais P., Garcia-Armisen T., George I., Billen G., 2007; Fecal bacteria in the rivers of the Seine drainage network (France): Sources, fate and modelling, *Science direct-ELSEVIER, Science of the Total Environment* **375**, pp. 152–167.

Steetsa B., Holden P., 2003; A mechanistic model of runoff-associated fecal coliform fate and transport through a coastal lagoon - Pergamon, *Water Research* **37**, pp. 589–608.

Swinbank W. C., 1963; Long-wave radiation from clear skies, *Quarterly Journal of the Royal Meteorological Society* **89**, pp. 339–348.

Taboada J. J., Prego R., Ruiz-Villarreal M., Montero P., Gómez-Gesteira M., Santos A., pérez Villar V., 1998; Evaluation of the seasonal variation in the residual patterns in the ría de vigo (NW Spain) by means of a 3D baroclinic model, *Estuarine, Coastal and Shelf Science* **47**, pp. 661–670.

Trancoso A. R., Saraiva S., Fernandes L., Pina P., Leitão P., Neves R., 2005; Modelling macroalgae using a 3d hydrodynamic-ecological model in a shallow, temperate estuary, *Ecological Modelling* **187**, pp. 232–246.

UNESCO, 1981; *Technic report on the joint panel on oceanographic tables and standards*, Technical papers in marine science 36, UNESCO, pp. 24.

USEPA, 1997; *Drinking Water Advisory: Consumer Acceptability Advice and Health Effects Analysis on MTBE*. # EPA-822-F-97-009. USEPA Office Of Water.

Vale C., Cortesão C. , Ferreira A., 1993; Suspended-sediment response to pulses in river flow and semidiurnal and fornightly tidal variations in a mesotidal estuary, *Marine Chemistry* **43,** pp. 21–31.

Vaz N., Dias J. M., Leitão P., Martins I., 2005ª; Horizontal patterns of water temperature and salinity in an estuarine tidal channel: Ria de Aveiro, *Ocean Dynamics* **55**, doi: 10.1007/s10236-005-0015-4, pp. 416–429

Vaz N., Dias J., Leitão P., Nolasco R., 2007; Application of the Mohid-2D model to a mesotidal temperate coastal lagoon, *Scince Direct, Computers & Geosciences* **33**, pp. 1204–1209.

Vaz N., Dias J., Leitão P., 2009; Three-dimensional modelling of a tidal channel: The Espinheiro Channel (Portugal), *Scince Direct, Continental Shelf Research* **29**, pp. 29–41.

Villarreal M. R., Montero P., Taboada J. J., Prego R., Leitão P. C., Péres-Villar V., 2002; Hydrodynamic model study of the ria de pontevedra under estuarine conditions, *Estuarine, Coastal and Shelf Science* **54 (1)**, pp. 101–113.

Wilkinson J., Jenkins A., Wyer M., Kay D., 1995; Modelling Faecal Coliform Dynamics in Streams and Rivers, *Elsevier Science Ltd.*, Great Britain, Pergamon, **Vol. 29**, No. 3, pp. 847-855.

Wollast R., Juillet 1978; *Rio Sado – Campagne de mesures: Rapport technique*, Laboratoire d'oceanographie de l' Université Libre de Bruxelles (para S.E.A.).

Outros online:

- http://www.thefreedictionary.com/ : The American Heritage® Dictionary of the English Language.
- http://www.thefreedictionary.com/ : Middle English, from Old English, *division of time*; see in Indo-European roots.
- http://www.switzerland.k12.in.us/watershed/fecal.html
- http://www.inag.pt/estuarios/
- http://www.aprh.pt/rgci/glossario/mare.html

ANNEX 1

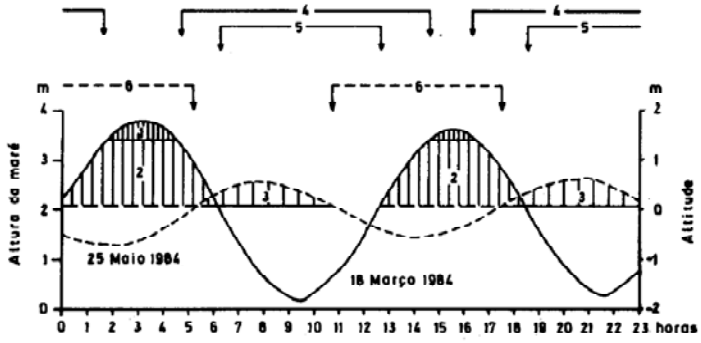

Fig. 6 — Ritmo diário da maré em águas vivas equinociais (curva a cheio, em 18 de Março de 1984) e em águas mortas equinociais (curva a tracejado, em 25 de Março de 1984), evidenciando-se os períodos de submersão e de emersão do sapal.

1 — Períodos de submersão do sapal alto em marés vivas; 2 — período de submersão do sapal baixo em marés vivas; 3 — período de submersão do sapal em marés mortas; 4 — período de emersão do sapal alto em marés vivas; 5 — período de emersão do sapal baixo em marés vivas; 6 — período de emersão do sapal baixo em marés mortas.

QUADRO I

Variação da altura da maré (em metros, acima do zero hidrográfico) registada no marégrafo de Tróia, segundo os valores apresentados nas Tabelas de Marés de 1981 a 1985

	Março	Junho	Média
Nível máximo da preamar viva	3,82	3,4	—
Nível médio da preamar viva	3,47	3,24	3,36
Nível médio da preamar morta	2,59	2,75	2,67
Nível médio da baixa-mar viva	0,46	0,63	5,45
Nível mínimo da baixa-mar viva	0,14	0,49	—
Nível médio da baixa-mar morta	1,27	1,09	1,18

Figure 26 - Variação da altura da Maré 1981-1985 (marégrafo de Tróia,) Source: Moreira M.J., 1987.

ANNEX 2

Table 12 - Principal astronomical components, periods (msd: solar day) and origin (PUGH, 1987).

Espécie	Componente	Período (msd)	Período (h)	Origem
0	S_a	364.96	8759.04	Solar anual
	S_{sa}	182.70	4384.80	Solar semianual
	Mm	27.55	661.20	Lunar mensal
	Mf	13.66	327.84	Lunar quinzenal
1	Q_1	1.12	26.88	Elíptica lunar maior
	O_1	1.08	25.82	Principal lunar
		1.04	24.84	Elíptica lunar menor
	M_1	1.04	24.84	Parallax lunar
		1.04	24.84	Elíptica lunar menor
	P_1	1.00	24.07	Principal solar
	S_1	1.00	24.00	Radiação
	K_1	1.00	23.93	Principal lunar
		1.00	23.93	Principal solar
	J_1	0.96	23.09	Elíptica lunar
2	N_2	0.53	12.65	Elíptica lunar menor
	M_2	0.52	12.43	Principal lunar
	L_2	0.51	12.19	Elíptica lunar menor
		0.51	12.19	Elíptica lunar menor
	T_2	0.50	12.02	Elíptica solar maior
	S_2	0.50	12.00	Principal solar
	R_2	0.50	11.98	Elíptica solar menor
	K_2	0.50	11.98	Declinação da lua
		0.50	11.98	Declinação do sol
3	M_3	0.35	8.28	Parallax lunar

Table 13 - Low waters harmonics, period and origin (PUGH, 1987).

Espécie	Componentes	Período (h)	Origem
Longo Período	Mm	661.20	$M_2 - N_2$
	Msf	354.37	$M_2 - S_2$
Diurna	MP_1	25.67	$M_2 - P_1$
	SO_1	22.42	$S_2 - O_1$
Semidiurna	MNS_2	13.13	$M_2 + N_2 - S_2$
	$2MS_2$	12.87	$2M_2 - S_2$
	MA_2	12.44	$2M_2 - S_a$
	MB_2	12.40	$2M_2 + S_a$
	MSN_2	11.79	$M_2 + S_2 - N_2$
	$2SM_2$	11.61	$2S_2 - M_2$
3-diurna	MO_3	8.39	$M_2 + O_1$
	MK_3	8.18	$M_2 + K_1$
4-diurna	MN_4	6.27	$M_2 + N_2$
	M_4	6.21	$M_2 + M_2$
	MS_4	6.10	$M_2 + S_2$
	MK_4	6.09	$M_2 + K_1$
	S_4	6.00	$S_2 + S_2$
6-diurna	M_6	4.14	$M_2 + M_2 + M_2$
	$2MS_6$	4.09	$2M_2 + S_2$
8-diurna	M_8	3.11	$4M_2$

ANNEX 3

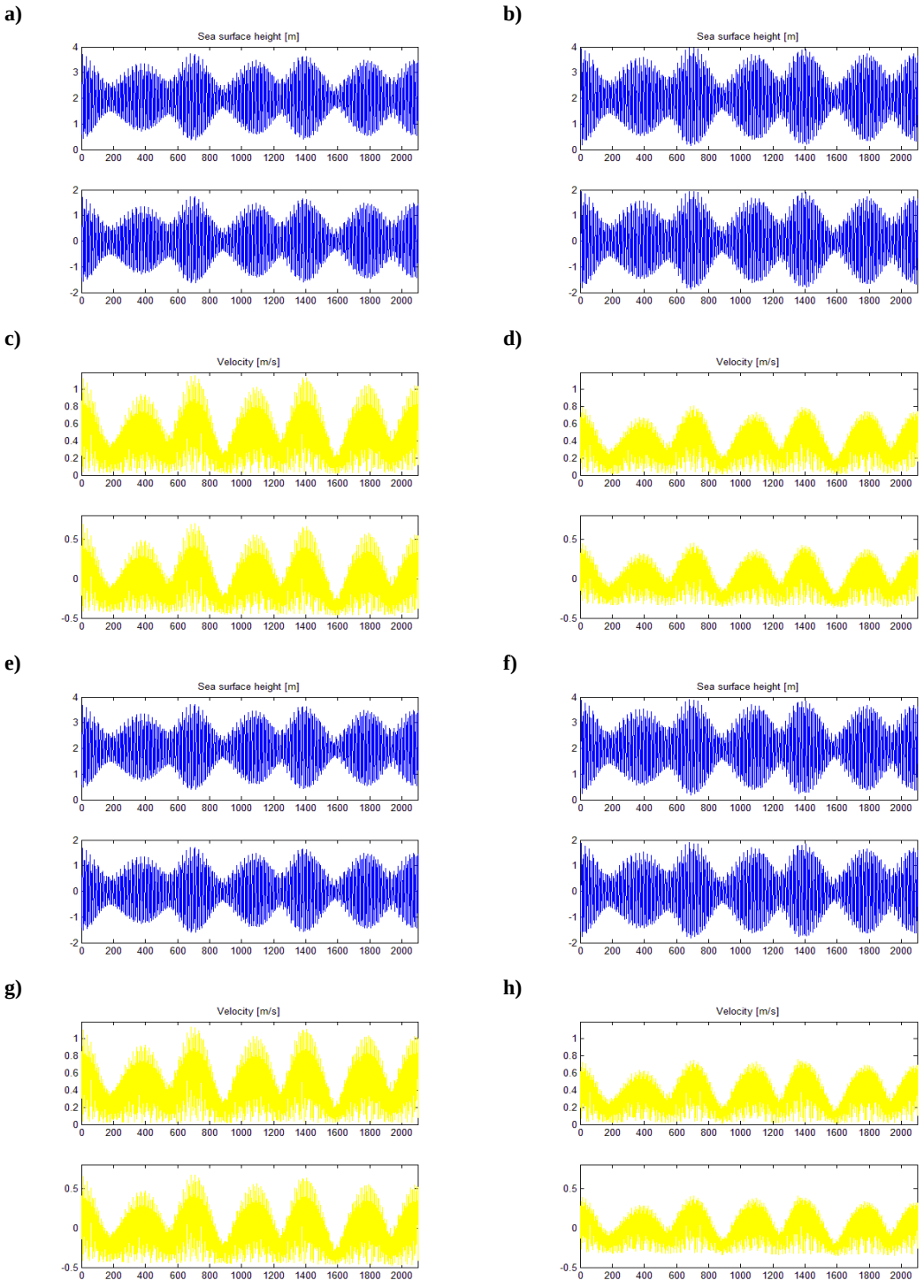

Figure 27 – Time series trend and mean removal: a) Station 1, Simulation 1, Q=200, r=0.0025, sea surface height, b) Station 4, Simulation 1, Q=200, r=0.0025, sea surface height , c) Station 1, Simulation 1, Q=200, r=0.0025, velocity, d) Station 4, Simulation 1, Q=200, r=0.0025, velocity, e) Station 1, Simulation 3, Q=200, r=0.0025, sea surface height, f) Station 4, Simulation 1, Q=200, r=0.0025, sea surface height, g) Station 1, Simulation 3, Q=200, r=0.0025, velocity, h) Station 4, Simulation 3, Q=200, r=0.0025, velocity.

ANNEX 4

Table 14 - Compilation of the last studies conducted in Sado estuary.

Actualização da avaliação do impacto da Central Térmica de Setúbal nos recursos halieuticos do Estuário do Sado	M. Antunes e P. Cunha	**1995**	INETI
Estuário do Sado : caracterização geral do ecosistema	Constancia Peneda, [et al.]	**1993**	INETI
Estado trófico e dinâmica do fitoplâncton das zonas superior, média e inferior do estuário do Sado	M. Oliveira e M. Coutinho	**1992**	INETI
Estudo do impacte dos efluentes urbano-industriais nas Comunidades de peixes e crustáceos decapodes no estuário do Sado 1987/88	Constancia Peneda, [et al.]	**1991**	INETI
Estudo da influência dos impactes antropogénicos na ecologia da ictiofauna e crustáceos decapodes no estuario do Sado 1989	Constancia Peneda, [et al.]	**1991**	INETI
Estuário do Sado: Contribuição para o conhecimento de características físicas e químicas : Campanhas de 1978-1980-1981 INII-LNETI	M. Santos Jorge	**1985**	INETI
Caracterização físico-química do estuário do Sado, em correlação com o efluente fabril do Centro de Produção Fabril de Setúbal de Portucel	S. Geada	**1981**	INETI
Avaliação do estado ambiental de um estuário de uso múltiplo, através da análise de Comunidades biosedimentares: Estuário do Sado	Ana Rodrigues	**1992**	INETI
Estuário do Rio Sado : Estudo Bacteriológico (1986-1990)	Lina Hall	**1994**	INETI
Caracterização físico-química das águas do estuário do rio Sado	Constancia Peneda [et al.]	**1991**	INETI
Contribuição para o estudo da poluição do estuário do rio Sado: I - Ensaios físicos e químicos	M. Rodrigues [et al.]	**1972**	INETI
General circulation in the lower Sado river estuary under drought conditions	Ambar *et al.*	**1980**	Article
Caracterização Hidrográfica do Estuário do Sado estuário do Sado	Ribeiro and Neves	**1982**	IST
Étude Experimentale et Modélisation des Circulations Transitoire et Résiduelle dans l'estuaire du Sado,	Neves	**1985**	Phd thesys
A Bidimensional Model for Residual Circulation in Coastal Zones. Application to the Sado Estuary	Neves	**1985**	Article